applied sciences

MDPI

Article

A New Approximate Analytical Solution for Coupled Mathieu-Type Differential Equations in Bridge and Vibrating Vehicle Suspension Interactions

Vytautas Kargaudas [1], Mindaugas Augonis [1,*] and Robertas Balevičius [2]

[1] Institute of Architecture and Construction, Kaunas University of Technology, LT44405 Kaunas, Lithuania; vytautas.kargaudas@ktu.lt
[2] Vilnius Gediminas Technical University, LT10223 Vilnius, Lithuania; robertas.balevicius@vilniustech.lt
* Correspondence: mindaugas.augonis@ktu.lt

Abstract

An energetic Lagrangian approach is applied to formulate coupled dynamic equations for unknown time-dependent displacements with respect to girder mid-span and vehicle suspension interaction, along with their rates and accelerations. The paper provides for a non-dimensional set of two linear non-homogeneous differential equations of a second order with variable coefficients, and a new analytical solution is proposed by implementing Lindstedt's singular perturbation method. This allowed us to obtain algebraic equations for girder mid-span displacement dynamic factors and suspension transmissibility coefficients vs. dimensionless time, three ratios of the loading frequency with respect to the girder and vehicle, and combined interaction frequencies related to free vibration. It is demonstrated that the derived system of Mathieu-type differential equations represents the free vibration problem of girder–suspension interaction subjected to the motion of a weightless vehicle, while four non-trivial fundamental solutions to the excitation of free-vibrating girder–suspension and suspension–girder systems are proposed. Simplified approximate analytical solutions are also given for dynamic factors of girder mid-span displacement. The analytically predicted results of dynamic variables are also compared with those determined numerically.

Keywords: girder mid-span displacement; dynamic factor; girder–suspension interaction; Mathieu's differential equation; moving load

Check for updates

Academic Editor: Sandro Carbonari

Received: 11 August 2026
Revised: 19 September 2026
Accepted: 25 September 2026
Published: 30 September 2026

Copyright: © 2026 by the authors. Licensee MDPI, Basel, Switzerland. This article is an open access article distributed under the terms and conditions of the Creative Commons Attribution (CC BY) license.

1. Introduction

Theoretical prediction of dynamic effects governed by the interaction of a moving vehicle with a bridge girder is of primary importance in bridge engineering and monitoring practice. There is also great demand for such theoretical prediction in the development of new approaches for accurate modeling of the serviceability limit state performance of existing bridges subjected to dynamic loads, and this demand has been substantially increasing over the past decades. This demand is mainly governed by the costliness of dynamic tests of the bridges. Meanwhile, bridge owners, stakeholders, and engineers face formidable tasks in terms of ensuring cost-efficient testing and monitoring techniques [1–3], interpreting data logically, and making timely decisions. Recently, indirect identifications of bridge modal parameters using data recorded from sensors mounted directly on a moving vehicle were considered in [1,4–7]. Meanwhile, comprehensive analysis, close-form solutions and advantages of using a two-axle asymmetric vehicle to scan the frequencies

of bridges have also been explored in [8]. However, the evolution of rotational modes due to the asymmetry of vehicle axles classically has a minimal effect with respect to the modal response of simple supported girders, since the rotational degree-of-freedom generated by energy components is usually small in terms of the total energy balance of the girder–vehicle system. These approaches provide an attractive, low-cost and simple-implementation alternative, but suffer in terms of accuracy [4] of the extracted modal parameters of the bridge, since the collected modal content should be properly decoupled from other vibration sources, e.g., road-surface-roughness-induced vibrations [5], etc.

Despite the fact that moving load problems are classical tasks of mechanics, their general solutions, attributed to deformable beams, are governed by mathematical complexity and difficulties even if the beam is modeled as a mechanical system with a maximally limited degree of freedom [9,10]. In this context, work by Mackertich [11,12] should be mentioned, where the dynamic response of a simply supported Timoshenko's beam is analyzed, including shear strains and the rotational effects of inertia. Meanwhile, the response of the Bernoulli–Euler beam to a moving mass is modeled by Fonda and Abduljabbar [13], where they implement a dynamic Green function. Some analytical and finite element method-based solutions to the beam response to the steady motion of a constant load have been discussed by Olsson [14].

The asymptotic behavior of the solution to the moving mass and moving oscillator of the Bernoulli–Euler beam has been analyzed by Pesterev et al. [15]. In contrast to the harmonic oscillations, the dynamic system response, exhibiting parametric oscillations, leads to mathematical complications [16,17]. Thus, when the periodicity of the constants in the linear differential equation of motion occurs, the general solution is governed by Mathieu's differential equation. Specifically, in the case of moving vehicle interaction with the bridge girder, its vertical displacements depend on free-vibration modes and are influenced by the free and loading vibrations of the vehicle suspension, which results in time-variable stiffness constants in dynamic equations. Despite the sufficient simplicity of Mathieu's differential equation in its canonical form [18], which depends on two parameters, a and q, there exists a non-closed-form analytical solution [19,20]. When the dynamic response of the system follows Mathieu's differential equation, parameter a can be related (in terms of the equation for the simple harmonic oscillations) to the natural frequency, while the q parameter can be recognized as the parametric excitation amplitude. Thus, the presence of this parameter produces the time-varying constant in Mathieu's equation, influencing the dynamic system response, or yielding its free vibrations, for $q = 0$. Moreover, depending on the combination of a and q values, tongue-like regions of unstable (unbounded) motion can be discerned graphically in so-called stability charts [21,22].

In finding an analytical solution to Mathieu's equation, most attempts [23], however, have yet to succeed, while numerical techniques serve as exact (or quasi-exact) and reliable approaches in terms of the first choice in the analysis. Major early contributions to the theoretical solutions to Mathieu's equation have been developed by relying on the application of the power series expansion method [16,17,23], which was originally introduced by Léonard Mathieu, when he discovered this equation. Then, Floquet developed a general method for the treatment of periodic coefficients by introducing Floquet's theorem, with its characteristic exponent allowing for obtaining *two linearly independent solutions*, while the introduction of the infinite determinants approach [16] proposed by Hill was the next achievement in finding solutions to Mathieu's equation. The periodic solution to Mathieu's differential equation, known as the Mathieu functions, provides a particular solution to this equation, with Whittaker introducing the integral equation, which explicitly affords a simple means of constructing even Mathieu functions [17]. In order to find a general solution to Mathieu's equation when the value of the periodic excitation amplitude q is

small, a *perturbation* method has been effectively applied [21,22]. It allows for using a two-variable expansion in power series (up to non-linear terms), which results in the equation of motion having the form of a simple harmonic oscillator in a rescaled time for one of the unknown variables. Since the general solution for harmonic oscillations is well known, its substitution for the second function of the variable in the differential equation allows for obtaining its solution along with the removal of resonant terms and the analysis of the $q(a)$ function values to consider the regions of unstable motions [22].

After Mathieu's equation was derived considering the oscillatory behavior of the vertical displacements of an elliptical drumhead, the presence of the cosine-based function of periodic excitation was found to be sufficiently characteristic in terms of describing a wide range of phenomena. In particular, a variety of problems in different fields associated with physics and mechanics can be accurately and realistically modeled by Mathieu's equation. In this case, structural dynamic responses depending on elliptical coordinates, electromagnetic wave guides, oscillations of water in a lake, the stability of floating bodies, Schrödinger's equation of quantum mechanics, etc. [19], can be mentioned among other parametric oscillators.

This paper presents a new analytical solution for a set of dynamic equations with time-variable coefficients for the case of the coupled interaction between the mid-span displacement of a bridge girder and moving vehicle suspension. It combines a particular solution for a set of non-homogeneous differential equations and a general solution for a set of homogeneous differential Mathieu-type equations. The solution proposes an analytical first-order perturbation prediction–correction approach to a general solution for the set of non-dimensional differential equations with an application of Lindstedt's singular perturbation method. In this case, the elimination of the secular terms is an important step in obtaining formulae of the eigenvalues of frequencies for the girder–suspension system. In this case, four non-trivial fundamental solutions for the excitation of the free-vibrating girder–suspension system are also presented. The solutions are important for a proper evaluation of the serviceability limit state in the design of new bridges and rehabilitation of existing bridges.

The original elements of the paper are as follows: (1) a new first-order perturbation analytical solution of two coupled Mathieu-type differential equations representing the coupled girder–suspension eigenvalues problem; (2) an approximate analytical solution for the vibrating girder and suspension vertical displacements, along with their rates and accelerations; (3) a simplified analytical solution for girder mid-span displacement with respect to the soft vibrating suspension interaction with the girder; (4) an alternative numerical method for solution of the set of dynamic equations accounting for any set of resultant forces acting on the vibrating mases.

Usually, the dynamic behavior of structures is predicted by measuring their dynamic response, upon which the structural modal or physical parameters are determined. In contrast, this study presents an approximate analytical solution of the bridge and vehicle interaction system characterized by periodic coupling properties.

2. The Dynamic Interaction Model and the Governing Equations

An idealized model of two lumped masses and springs and a viscous dashpot (Figure 1) is considered in terms of an analytical solution for girder mid-span and suspension vertical displacement.

An energetic Lagrangian approach will be implemented below for a derivation of the governing equations of the model for the case of the non-viscous response of the girder. In this case, only conservative forces are considered to allow us to derive the motion equations suitable for an analytical solution.

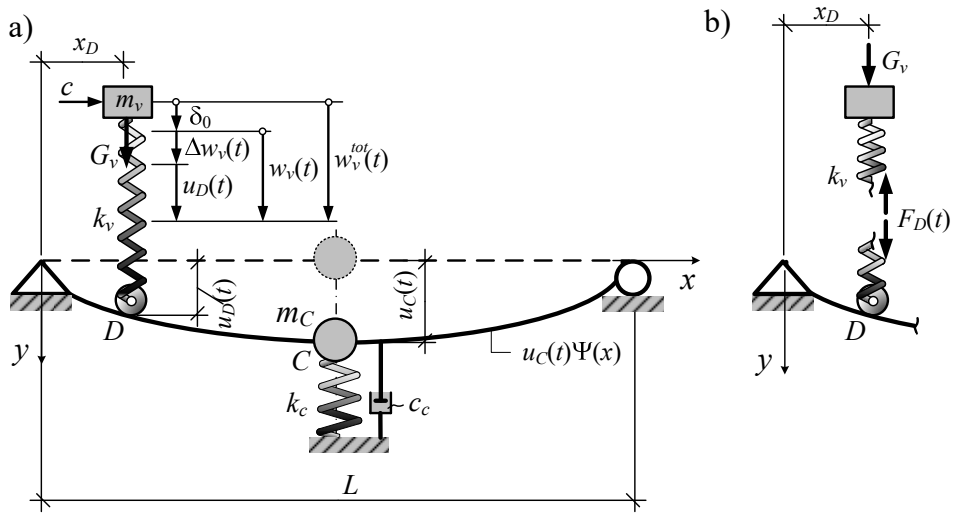


Figure 1. Idealized model of the bridge girder and vehicle interaction (**a**) and internal vehicle suspension force (**b**).

A simply supported bridge girder *mid-span* displacement u_C is considered under the steady motion of a vehicle with total mass m_V over the L span of the bridge. The horizontal speed of the vehicle is defined by vector c, while the motion of its suspension is idealized via an elastic spring with an *effective* stiffness constant k_V as the whole vehicle. In this case, the previously proposed micro-mechanical wheel and spherical asperity interaction model [20] is not applied to simplify the dynamic equations for the possibility of analytical solution.

The total weight load of the vehicle (including the suspension weight and other weights) equals $G_V = m_V g$, where g is gravity acceleration. The static displacement of the suspension is $\delta_0 = G_V/k_V$ (Figure 1).

For the steady motion of the vehicle over the girder, any position $x_D = ct$ at time instant t is considered. The total vertical displacement of the vehicle suspension is measured from the initial (undeformed) state and equals $w_V^{tot}(t) = \delta_0 + \Delta w_V(t) + u_D(t)$ (Figure 1). Here, $\Delta w_V(t)$ stands for the relative dynamic displacement (i.e., elongation or shortening) of the suspension spring at t, measured from the position of static equilibrium. The function $u_D(t)$ is the vertical displacement of the girder at vehicle position x_D (Figure 1), which is measured from the static equilibrium position of the girder (i.e., the displacement of the girder due to its own weight is not considered).

A relative displacement, $\delta_0 + \Delta w_V(t)$, generated at point D (Figure 1), induces the internal force $F_D(t) = k_V(\delta_0 + \Delta w_V(t))$ in the suspension spring. As can be seen in Figure 1, the relative displacement of the suspension spring equals $\delta_0 + \Delta w_V(t) = w_V^{tot}(t) - u_D(t) = w_V(t) + \delta_0 - u_D(t)$, where $w_V(t)$ is the vertical dynamic displacement of the suspension.

At time t, developed girder displacement $u_D(t)$ also exerts a spring force on point C of the girder. Meanwhile, their interaction with respect to the simply supported girder is supposed to be under a displacement shape function corresponding to a first fundamental vibration mode, i.e., $\Psi(x) = \sin\left(\frac{\pi x}{L}\right)$, and, in turn, $u_D(t) = u_C(t)\Psi(x_D) = u_C(t)\sin\theta t$ (where $\theta = \frac{\pi c}{L}$ is the *loading frequency* due to the moving vehicle on the bridge girder). In this case, the pre-defined shape of displacements leads to avoiding a solution of the partial differential equation with respect to finding two-dimensional function $u_C(t,x)$. This approximation predicting the mid-span displacement evolution in time due to a moving load provides small errors, while a fundamental first mode of vibration takes place in sufficiently stiff girders, such as those found in reinforced concrete bridges.

The internal force $F_D(t)$ acting on the suspension spring at t is transferred to the girder as an opposite-direction load via an idealized wheel model (Figure 1b). This induces the unknown girder's mid-span displacement $u_C(t)$ at t. Then, the girder's spring force (point C

in Figure 1) is equal to the resultant force $F_C(t) = F_{CD}(t) - k_c u_C(t)$, where $k_c = \frac{48EI}{L^3}$ stands for the girder spring constant assessing flexural stiffness EI of the girder's cross-section, and $F_{CD}(t) = F_D(t)\Psi(x_D)$ is the girder load at point C exerted by vehicle suspension force $F_D(t)$ acting at point D (Figure 1). Note that the dashpot force is excluded from the resultant force with respect to the further analytical solution. Only the *relative* displacement deforms the spring of the vehicle suspension and the spring of the girder. Consequently, the *stored* energy due to elastic deformation in the suspension spring simply equals $\frac{1}{2}k_V(\delta_0 + \Delta w_V)^2$, while in the girder spring, it is $\frac{1}{2}k_c u_C^2$. Meanwhile, the potential energy due to the action of weight force G_V in the gravitational field is equal to $G_V(0 - (\delta_0 + w_V))$. Hence, the whole potential energy of the vehicle–girder system is expressed, in Figure 1a, as:

$$\Pi = \frac{1}{2}k_c u_C^2 + \frac{1}{2}k_V(\delta_0 + w_V - u_C \sin\theta t)^2 - G_V(\delta_0 + w_V). \quad (1)$$

The girder–vehicle system's kinetic energy equals to $T = \frac{m_C \dot{u}_C^2}{2} + \frac{m_V \dot{w}_V^2}{2}$.

Thus, the Lagrangian is $L = T - \Pi$, and Lagrange's equations for $\frac{d}{dt}\left(\frac{\partial L}{\partial \dot{u}_C}\right) = \frac{\partial L}{\partial u_C}$ and $\frac{d}{dt}\left(\frac{\partial L}{\partial \dot{w}_V}\right) = \frac{\partial L}{\partial w_V}$ give the following set of equations of motion:

$$\begin{cases} m_C \ddot{u}_C = -k_c u_C + k_V(\delta_0 + w_V - u_C \sin\theta t)\sin\theta t \\ m_V \ddot{w}_V = -k_V w_V + k_V u_C \sin\theta t \end{cases} \quad (2)$$

Here, m_C is the effective (i.e., lumped) bridge girder mass, calculated by dividing the bridge into two parts and attaching a half-part of the mass at the ends of each part [24]; thus, $m_C \equiv m_{C,eff} = \frac{1}{2}m$, where m is the total bridge girder mass.

Finally, after some rearrangements, the set in Equation (2) can be written in the following form:

$$\begin{cases} m_C \ddot{u}_C + k_C u_C = (G_V - m_V \ddot{w}_V) sin\theta t, \\ m_V \ddot{w}_V + k_V w_V = k_V u_C sin\theta t. \end{cases} \quad (3)$$

The set in Equation (3) represents the system of linear non-homogeneous differential equations of a second order for unknown displacement $u_C(t)$, expressing the *static and dynamic* response of the girder at mid-span and unknown *dynamic* displacement $w_V(t)$ of the vehicle suspension, when the vehicle moves over the bridge at constant speed c (Figure 1). The first and second derivatives (denoted by dots) of these variables provide their velocities and accelerations, respectively.

In general, the obtained bridge–vehicle interaction equations provide an insight into the phenomenon of oscillatory load transfer from the moving vehicle suspension to the bridge girder. In particular, from the vertical motion equation of the vehicle suspension mass, the girder mid-span displacement can be decomposed into two displacements, $-u_C(t) = \frac{\Phi_V(t)}{\sin(\theta t)k_V} - \frac{w_V(t)}{\sin(\theta t)}$, where $\Phi_V(t) = -m_V \ddot{w}_V(t)$ is the inertial force of the suspension. It specifies that the girder mid-span displacement is composed of the displacement induced by vehicle suspension inertia force Φ_V and suspension dynamic displacement w_V transferred to the simply supported girder, vibrating under the first mode. As Φ_V and w_V are functions of the oscillatory character, resulting from the free vibrating frequencies of the girder, suspension and loading frequency, the final evolution of $u_C(t)$ is generated by competitive composition of Φ_V and w_V functions. In this case, $t = 0$, $u_C(t)$ is not singular, and $u_C(0) = 0$, as follows from the L'Hôpital rule for zero initial values of all functions.

Meanwhile, the motion of the lumped mass of the girder is subjected to vehicle suspension weight force G_V counteracted by development of suspension inertial force $\Phi_V(t) = -m_V \ddot{w}_V(t)$ with time.

3. A Non-Dimensional Form of Differential Equations

For a further analytical solution, it is convenient to express the equations in a non-dimensional form. In this case, we introduce a new variable, $\xi = \theta t$, which leads to π-times rescaled *dimensionless* time variable $\frac{t}{t_u}$, i.e., $\xi = \pi\frac{t}{t_u}$, where $t_u = \frac{L}{c}$ is the time the vehicle takes to pass the bridge girder. By replacing this variable in set (3), the first equation can be rewritten in the following way:

$$\frac{m_C}{k_C}\ddot{u}_C + u_C = \frac{G_V}{k_C}\left[1 - \frac{m_V\ddot{w}_V}{G_V}\right]\sin\xi. \tag{4}$$

The differential of the rescaled time variable equals to $d\xi = \theta dt$, while, when squared up, it gives $dt^2 = \frac{1}{\theta^2}d\xi^2$. Now, let the new variables w and u have the derivatives, which are related to the rescaled time as follows:

$$\ddot{w} = \frac{d^2w}{d\xi^2} = w'', \ \ddot{u} = \frac{d^2u}{d\xi^2} = u''. \tag{5}$$

Referring to Equations (4) and (5), the girder mid-span and vehicle suspension displacements can be expressed in terms of the new variables as:

$$u_C = \frac{G_V}{k_C}u, \ w_V = \frac{G_V}{k_C}w. \tag{6}$$

Hence, $u = \frac{u_C}{u_C^0}$ specifies the dimensionless variable defining the time-varying evolution of the dynamic factor of girder mid-span displacement, where $u_C^0 = \frac{G_V}{k_C}$ stands for girder mid-span displacement due to the static application of load G_V (Figure 1). Its maximal values $D_u = \frac{\max u_C(t)}{u_C^0} \equiv \max u(\xi)$ will be analyzed below as they are important in bridge design and monitoring. Meanwhile, $w = \frac{w_V}{u_C^0}$ can be referred to as the transmissibility factor (a dimensionless variable) of the vehicle suspension when it travels over the girder at a constant speed.

Using Equations (5) and (6), the accelerations of girder mid-span and vehicle suspension displacements vs. rescaled time are given as:

$$\ddot{u}_C = u_C^0\frac{du^2}{dt^2} = u_C^0\frac{du^2}{d\xi^2}\theta^2 = u''\theta^2u_C^0, \tag{7}$$

$$\ddot{w}_V = u_C^0\frac{dw^2}{dt^2} = u_C^0\frac{dw^2}{d\xi^2}\theta^2 = w''\theta^2u_C^0. \tag{8}$$

Hence, when we apply these formulae to Equation (4), they can be rewritten in terms of dimensionless variables, as follows:

$$\frac{m_C}{k_C}\theta^2\frac{G_V}{k_C}u'' + \frac{G_V}{k_C}u = \frac{G_V}{k_C}\left[1 - \frac{m_V}{G_V}\theta^2\frac{G_V}{k_C}w''\right]\sin\xi = \frac{m_C}{k_C}\theta^2u'' + u = \left[1 - \frac{m_V}{k_C}\theta^2w''\right]\sin\xi \tag{9}$$

Finally, we can introduce the coefficients accounting for the ratios of frequencies $\mu_0 = \theta^2\frac{m_V}{k_C} = \mu_1\frac{m_V}{m_C}$ and $\mu_1 = \theta^2\frac{m_C}{k_C} = \frac{\theta^2}{\omega_C^2}$ in Equation (9), and $\mu_2 = \theta^2\frac{m_V}{k_V} = \frac{\theta^2}{\omega_V^2}$ in the second equation of set (3). Here, ω_C^2 and ω_V^2 are the natural vibration frequencies of the girder and vehicle suspension, respectively. Thus, we arrive now at the following system of differential equations:

$$\begin{cases} \mu_1u'' + u = [1 - \mu_0w'']\sin\xi \\ \mu_2w'' + w = u\sin\xi \end{cases}. \tag{10}$$

where $u'' = \frac{d^2u}{d\xi^2}$ and $w'' = \frac{d^2w}{d\xi^2}$ are dimensionless derivatives vs. rescaled time variable ξ'.

The derived system of differential equations represents the non-dimensional form of motion Equation (2) for the unknown functions of dynamic factor $u(\xi)$ of girder mid-span displacement and vehicle suspension transmissibility factor $w(\xi)$ in dimensionless time ξ.

4. Approximate Analytical Solutions of Differential Equations

4.1. A System of Homogeneous Equations

In the set of differential Equation (10), frequency ratios $\mu_1 = \frac{\theta^2}{\omega_C^2}$ and $\mu_2 = \frac{\theta^2}{\omega_V^2}$ define the dynamics of the bridge girder and vehicle suspension, while frequency ratio $\mu_0 = \theta^2 \frac{m_V}{k_C} = \mu_1 \frac{m_V}{m_C}$ couples their interaction. Moreover, if $\mu_0 = 0$, the equations in system (10) can be resolved independently.

In set (10), the differential equations are linear non-homogeneous equations of a second order due to the presence of 1 in the brackets of the first equation. Mathematically, the solution of the non-homogeneous differential equation combines the general solution of the homogeneous equation and any particular (non-trivial) solution of the non-homogeneous equation. Indeed, the particular solution of Equation (10) is quite straightforward. However, the solution of *homogeneous* differential equations in system (10) is complicated. In particular, the homogeneous equations in (10) can be written as:

$$\begin{cases} \mu_1 u'' + u = -\mu_0 w'' sin\xi, \\ \mu_2 w'' + w = usin\xi. \end{cases} \tag{11}$$

In general, the differential equations in (11) represent coupled Mathieu-type differential equations, with the periodicity of coefficients resulting in parametric oscillatory behavior. Specifically, set (10) presents coupled Mathieu-type-forced differential equations.

Specifically, in this set, two motion equations are governed by trigonometric function $\sin\xi$, whose multiplication by girder and vehicle suspension spring constants k_c and k_V leads to their cosine (sine) periodically varying spring stiffness coefficients:

$$\left(1 + \frac{k_V}{k_c}\sin^2\xi\right) k_c u_C = \left(\underbrace{1 + \overbrace{\frac{k_V}{2k_c}}^{q}}_{a} - \underbrace{\frac{k_V}{2k_c}}_{q} \cos 2\xi \right) k_c u_C,$$

$$(a - q\cos 2\xi)^{-1} k_V w_V \approx (a + q\cos 2\xi)\, k_V w_V,$$

where $a(q) = 1 + q$ and $q = \frac{k_V}{2k_c}$ are the parameters of the canonical form of Mathieu Equation (35). Notably, the approximate formula is applicable to small values of stiffness ratio $q \ll 1$.

The solutions for Mathieu's equations have been extensively studied by Erdelyi et al. [16]. In this case, for the solution of Equation (11), unknown functions $u(\xi)$ and $w(\xi)$ can be represented by the infinite Laurent series $u = \sum_{-\infty}^{+\infty} a_n e^{(\vartheta + ni)\xi}$, $u = \sum_{-\infty}^{+\infty} a_n e^{(\vartheta + ni)\xi}$ and $w = \sum_{-\infty}^{+\infty} b_n e^{(\vartheta + ni)\xi}$, where a_n and b_n are unknown coefficients, while $i = \sqrt{-1}$ stands for an imaginary unit. Indeed, for $\vartheta = 0$, the Laurent series is equivalent to Fourier's series in an exponential form.

After substituting this series into Equation (11) and using Euler's formula $sin\xi = \frac{i}{2}\left(e^{-i\xi} - e^{i\xi}\right)$, two recurrence algebraic equations connecting coefficient b_n with a_{n+1} and a_{n-1} and a_n with b_{n+1} and b_{n-1} can be obtained. Thus, we can define the sequence of the infinite number of *linear* homogeneous algebraic equations for $n = 0, \pm 1, \pm 2, \ldots, \pm\infty$ to determine the unknown periodic coefficients satisfying Equation (11). In particular, coefficients $a_0, a_{\pm 1}, a_{\pm 2}, \ldots$ and coefficients $b_0, b_{\pm 1}, b_{\pm 2}, \ldots$ can be found separately using the same system of algebraic equations, when the system's determinant $\Delta(\vartheta_0)$, depending

on the unknown constant ϑ, is equal to zero, i.e., $\Delta(\vartheta_0) = 0$, which represents a *meromorphic* function of ϑ.

The formation of the infinite determinant of the systems of equations and solutions is described by Erdelyi et al. in [16] and by Whittaker and Watson in [17]. However, as is pointed out in [16], the calculation of the root ϑ_0 of the determinant raises only the first difficulty, among others, in determining the Mathieu functions required. Similarly, our analysis has allowed for obtaining the root of *meromorphic* function $\Delta(\vartheta_0)$; however, in the large range of coefficient ϑ values, (especially at root ϑ_0), determinant $\Delta(\vartheta_0)$ was only approaching zero, but not equal to it. Due to this, the prediction of coefficients a_0, $a_{\pm1}$, $a_{\pm2}$, ... became practically impossible despite the fact that they do exist theoretically.

Consequently, rather than applying the infinite determinant prediction approach for the solution of differential equations in set (11), we shall introduce a new approximate solution based on the analytical prediction–correction approach and Lindstedt's singular perturbation method.

4.1.1. Representation of Constants

Lindstedt's method represents a *singular perturbation* scheme, where a key step for the removal of the resonant or *secular* terms is effectively applied in [21]. The main principles of this approach will be implemented below.

In this case, for small values of constant μ in differential equations, let μ_j (j = 1.2) be expanded by a power series. For a first order perturbation scheme, retaining only linear terms in the series and omitting $O\left(\mu_j^2\right)$, the coefficients in Equation (11) are expressed by applying the multiplier "1" for variables u and w, as follows:

$$\begin{cases} \mu_j = q_{j0} + q_{j1}\varepsilon, \\ 1 = p_{j0} + p_{j1}\varepsilon, j = 1.2. \end{cases} \tag{12}$$

Here, terms q and p are unknown, while ε stands for any real number, $\varepsilon < 1$. Similarly, the unknown functions u and w, as in the solution to Equation (11), are also represented by the power series using only linear terms without $O(\varepsilon^2)$:

$$u = u_0 + \varepsilon u_1, w = w_0 + \varepsilon w_1. \tag{13}$$

where u_0, u_1 and w_0, w_1 are the *first* and *second* approximations of u and w functions, respectively.

Then, by setting $\varepsilon = 0$ and substituting Equations (12) and (13) into Equation (11), we get a general set of differential equations for the *first* approximation of the solution:

$$\begin{cases} q_{10}u_0'' + p_{10}u_0 = 0, \\ q_{20}w_0'' + p_{20}w_0 = u_0 sin\xi. \end{cases} \tag{14}$$

The second approximation is obtained by using the same equation applying ε, which is expressed from Equation (12) and then substituted into Equation (13) along with the final application to Equation (11):

$$\begin{cases} q_{10}u_1'' + p_{10}u_1 = -kw_0'' sin\xi - q_{11}u_0'' - p_{11}u_0, \\ q_{20}w_1'' + p_{20}w_1 = u_1 sin\xi - q_{21}w_0'' - p_{21}w_0. \end{cases} \tag{15}$$

In this set, constant μ_0 from Equation (11) is replaced by $\mu_0 = k\varepsilon$, where k is any number close to a unit (e.g., if k = 1, then $\varepsilon \equiv \mu_0$).

In the equations of the first approximation (14), constants q_{10} and q_{20} are assumed to represent a certain generalized mass, while p_{10} and p_{20} are supposed to be the generalized

stiffness constants of the springs, since the first equation of Equation (14) represents the equation of the free vibrations of the girder, while the second equation can be provided for the *harmonic* (or periodic in a more general sense) excitation of the suspension. In this case, the frequencies are simply expressed from Equation (14) as:

$$\lambda = \sqrt{\frac{p_{10}}{q_{10}}},\ \eta = \sqrt{\frac{p_{20}}{q_{20}}}. \tag{16}$$

The set in Equation (12) and functions in Equation (13) converge when

$$n_1 = \frac{q_{21}}{q_{20}}\varepsilon \text{ and } n_2 = \frac{p_{21}}{p_{20}}\varepsilon$$

are $n_1 > n_2$, and $|n_1| \ll 1$ and $|n_2| \ll 1$. Thus, from the minimal condition $\min\left(n_1^2 + n_2^2\right)$, the equations for predicting the unknown constants in the set of first and second approximations can be expressed as:

$$q_{20} = \frac{1}{\eta^2}\frac{\mu_2^2\eta^4 + 1}{\mu_2\eta^2 + 1},\ q_{21} = \frac{1}{\varepsilon\eta^2}\frac{\mu_2\eta^2 - 1}{\mu_2\eta^2 + 1},\ p_{20} = \frac{\mu_2^2\eta^4 + 1}{\mu_2\eta^2 + 1},\ p_{21} = \frac{\mu_2\eta^2}{\varepsilon}\frac{1 - \mu_2\eta^2}{1 + \mu_2\eta^2} \tag{17}$$

The same formulae can be applied to get constants q_{10}, q_{11}, p_{10}, and p_{11}, when λ is substituted for η in Equation (17), and μ_2 is replaced by μ_1. Finally, the solution of the first equation for the free-vibrating motion in Equation (14) is independent of the second equation, which yields that the second equation can be resolved subsequently. Hence, the solution of the *first* approximation for unknown functions u_0 and w_0 leads to the following formulae:

$$\begin{cases} u_0 = 4(A_1 cos\lambda\xi + A_2 sin\lambda\xi), \\ w_0 = 4(B_1 cos\eta\xi + B_2 sin\eta\xi) + \frac{2}{q_{20}P_{1-}}(A_2 cos(\lambda-1)\xi - A_1 sin(\lambda-1)\xi) \\ + \frac{2}{q_{20}P_{1+}}(A_1 sin(\lambda+1)\xi - A_2 cos(\lambda+1)\xi), \end{cases} \tag{18}$$

where $P_{j\pm} = \eta^2 - (\lambda \pm j)^2$, $j = 1, 2, 3, \ldots$, and A_1, A_2, B_1, and B_2 are arbitrary constants satisfying the appropriate initial conditions for $\xi = 0$.

By substituting the solutions (18) into the right side of both equations of set (15), we can obtain solutions for functions u_1 and w_1 of the second approximation as sums of harmonic terms. In this case, after the substitution, at the right side of the obtained equations, we get the secular terms, such as $\xi sin\lambda\xi$ or $\xi sin\eta\xi$. In general, when $\xi \to \infty$, the amplitude of the second approximation also increases indefinitely, resulting in an unbounded motion [22]. Following Lindstedt's approach, these secular (resonant) terms should be set equal to zero. Finally, after mathematical rearrangements, this yields the following equations for the second approximation:

$$\begin{gathered} u_1 = 2A_3 cos\lambda\xi + 2A_4 sin\lambda\xi - 2h_-(A_1 cos(\lambda-2)\xi + A_2 sin(\lambda-2)\xi) \\ +2h_+(A_1 cos(\lambda+2)\xi + A_2 sin(\lambda+2)\xi) + 2h_-^*(B_2 cos(\eta-1)\xi - B_1 sin(\eta-1)\xi) \\ +2h_+^*(B_1 sin(\eta+1)\xi - B_2 cos(\eta+1)\xi); \end{gathered} \tag{19}$$

$$\begin{gathered} w_1 = B_3 cos\eta\xi + B_4 sin\eta\xi + \frac{h_+^*}{4q_{20}(\eta+1)}(B_1 cos(\eta+2)\xi + B_2 sin(\eta+2)\xi) \\ -\frac{h_-^*}{4q_{20}(\eta-1)}(B_1 cos(\eta-2)\xi + B_2 sin(\eta-2)\xi) + \frac{1}{q_{20}P_{1-}}(A_4 cos(\lambda-1)\xi - A_3 sin(\lambda-1)\xi) \\ +\frac{1}{q_{20}P_{1+}}(A_3 sin(\lambda+1)\xi - A_4 cos(\lambda+1)\xi) + \frac{h_- + 2s_-}{q_{20}P_{1-}}(A_2 cos(\lambda-1)\xi - A_1 sin(\lambda-1)\xi) \\ +\frac{h_+ - 2s_+}{q_{20}P_{1+}}(A_2 cos(\lambda+1)\xi - A_1 sin(\lambda+1)\xi) + \frac{h_-}{q_{20}P_{3-}}(A_1 sin(\lambda-3)\xi - A_2 cos(\lambda-3)\xi) \\ +\frac{h_+}{q_{20}P_{3+}}(A_1 sin(\lambda+3)\xi - A_2 cos(\lambda+3)\xi), \end{gathered} \tag{20}$$

where A_3, A_4, B_3, and B_4 are arbitrary constants satisfying the initial conditions for $\xi = 0$, $h_{\pm} = k\frac{\lambda\pm1}{8q_{10}q_{20}P_{1\pm}}$, for $P_{1\pm} \neq 0$, and $h_{1\pm} = 0$, for $k = P_{1\pm} = 0$; $h^*_{\pm} = k\frac{\eta^2}{q_{10}\left(\lambda^2-(\eta\pm1)^2\right)}$, for $\lambda^2 \neq (\eta \pm 1)^2$, and $h^*_{1\pm} = 0$, for $k = \lambda^2 - (\eta \pm 1)^2 = 0$; $s_{\pm} = \frac{q_{21}(\lambda\pm1)^2-p_{21}}{q_{20}\left(\eta^2-(\lambda\pm1)^2\right)}$, for $\eta^2 \neq (\lambda \pm 1)^2$, and $s_{\pm}$=0, for $q_{21}(\lambda \pm 1)^2 - p_{21} = \eta^2 - (\lambda \pm 1)^2 = 0$; and $P_{3\pm}$=$\eta^2 - (\lambda \pm 3)^2$.

The obtained equations of the second approximation of the solution for the set of homogeneous differential equations in Equation (11) for dynamic factor u_1 of mid-span displacement and vehicle transmissibility factor w_1 correct the prediction of the first approximation for u_0 and w_0 given by Equation (18). The solution operates with the constants $A_1, \ldots A_4$ and $B_1, \ldots B_4$, which can be expressed by applying the initial conditions for u and w.

4.1.2. Prediction of Frequencies

In Equations (19) and (20), the frequency ratios given by Equation (16) should be now determined and related with frequency ratios μ_0, μ_1, and μ_2. In this case, we apply the conditions on the absence of secular terms in Equations (19) and (20):

$$\begin{cases} \frac{\mu_0}{4}\left[\frac{(\lambda+1)^2}{\eta^2-(\lambda+1)^2} + \frac{(\lambda-1)^2}{\eta^2-(\lambda-1)^2}\right] = q_{20}\left(1-\mu_1\lambda^2\right),\ \eta^2 \neq (\lambda\pm1)^2 \\ \frac{\mu_0}{4}\left[\frac{\eta^2}{\lambda^2-(\eta+1)^2} + \frac{\eta^2}{\lambda^2-(\eta-1)^2}\right] = q_{10}\left(1-\mu_2\eta^2\right),\ \lambda^2 \neq (\eta\pm1)^2. \end{cases} \quad (21)$$

These algebraic equations are non-linear for unknowns λ and η and satisfy several roots. For further calculations, only one pair of the roots, such as $\lambda \to \lambda_0$ and $\eta \to \eta_0$ (when $\mu_0 \to 0$, and the terms in the square brackets are not equal to zero), is feasible. Here, $\lambda_0 = \frac{1}{\sqrt{\mu_1}} = \frac{\omega_C}{\eta}$ and $\eta_0 = \frac{1}{\sqrt{\mu_2}} = \frac{\omega_V}{\eta}$ can be treated as the limit values of frequency ratios for Equations (11) and (21). From Equation (21), unknowns λ and η can be resolved iteratively by applying the classical Newton step approach in terms of selecting the initial guess values to be equal to λ_0 and η_0.

The roots λ and η are dimensionless parameters and serve as rescaling factors for the frequencies of mechanical systems $\lambda\theta$ and $\eta\theta$, respectively.

If $\xi = 0$, the vehicle position is at the initial point of the bridge girder, and we can simply get separated equations for free vibrations of the girder and the vehicle suspension ($\mu_1 u'' + u = 0$ and $\mu_2 w'' + w = 0$, respectively). If the vehicle stands at any position $x = \alpha$, then $sin\xi = \alpha = const$. Then the system of Equation (11) rearranges as:

$$\begin{cases} \mu_1 u'' + u = -\mu_0 \alpha w'', \\ \mu_2 w'' + w = \alpha u \end{cases}$$

In this case, a substitution of u from the second equation into the first equation of the system yields

$$\mu_1\mu_2 w^{(IV)} + (\mu_1 + \mu_2 + \alpha^2\mu_0)w'' + w = 0.$$

If λ and η are close to λ_0 and η_0, the following approximate equations are derived from the classical Newton iterative approach:

$$\lambda \approx \lambda_0\left(1 - \frac{\mu_0}{4\mu_2}\frac{K_1}{2}\right),\ \eta \approx \eta_0\left(1 + \frac{\mu_0}{4\mu_1}\frac{K_2}{2}\right),\ K_1 = \frac{(\lambda_0+1)^2}{\eta_0^2-(\lambda_0+1)^2} + \frac{(\lambda_0-1)^2}{\eta_0^2-(\lambda_0-1)^2},\ K_2 = \frac{\eta_0^2}{(\eta_0+1)^2-\lambda_0^2} + \frac{\eta_0^2}{(\eta_0-1)^2-\lambda_0^2}.$$

Moreover, we can apply the conditional vehicle positions, such as $\alpha_\lambda = sin\xi_\lambda$ and $\alpha_\eta = sin\xi_\eta$, and then obtain the true corrected λ and η values. Here, the parameters are $\alpha_\lambda = \frac{\mu_1-\mu_2}{\mu_1+\mu_2}\frac{K_1}{2}$ and $\alpha_\eta = \frac{\mu_1-\mu_2}{\mu_1+\mu_2}\frac{K_2}{2}$.

Theoretically, let us analyze the fundamental solutions of Equation (11). Thus, the homogeneous system of Equation (11) has one *trivial* solution, $u \equiv w \equiv 0$, and four *non-trivial fundamental* solutions (13), where u_0, w_0, u_1 and w_1 are fundamental solutions (18), (19), and (20). These fundamental solutions are of a similar nature with respect to the free vibrations of a mechanical system, when the differential equation is defined with constant coefficients. In this case, the solution is classically based on the combination of sine and cosine functions, with their arguments depending on the natural frequencies. When the differential equations are with time-variable (periodic) coefficients, then the fundamental solutions are functions, which can be approximated by a sum of the harmonics, such as Equations (13) and (18)–(20). Applied frequencies λ and η are not natural frequencies of the mechanical system, since in the solutions of Equations (18)–(20), we have applied a system of different frequencies. In particular, the mechanical sense of the vibrations in Equation (11) represents the case of the vibration of the bridge girder under the motion of a *weightless* vehicle, when $G_V = 0$ (cf. Equation (3)).

This implies that if $G_V = 0$, then and only then do the trivial solutions $u_c(t) \equiv 0$ and $w_V(t) \equiv 0$ exist in Equation (3). Thus, in the mechanical system of bridge girder–vehicle suspension with $G_V = 0$, if at initial time instant $t_0 = 0$ the vertical displacement of the vehicle suspension is not zero, only then does the whole system come into motion. Four different solutions of the mechanical system response, when its initial values are

$$\begin{cases} u(0) = 1,\ u'(0) = 0,\ w(0) = 0,\ w'(0) = 0, \\ u(0) = 0,\ u'(0) = 1,\ w(0) = 0,\ w'(0) = 0, \\ u(0) = 0,\ u'(0) = 0,\ w(0) = 1,\ w'(0) = 0, \\ u(0) = 0,\ u'(0) = 0,\ w(0) = 0,\ w'(0) = 1, \end{cases} \tag{22}$$

give the system of the initial conditions. These solutions can be interpreted as the solutions for the eigen vibrations of the girder–vehicle system. In particular, when $\mu_0 \to 0$ (where $\mu_0 = \theta^2 \frac{m_V}{k_C} = \mu_1 \frac{m_V}{m_C}$), all fundamental solutions approach the case of free vibrations of the vehicle suspension or free vibrations of the girder with no interaction.

In Figure 2, the results of four fundamental solutions for u and w from the system of homogeneous differential equations are plotted accounting for the set of initial conditions (22). Using this set, arbitrary constants $A_{1\ldots4}$ and $B_{1\ldots4}$ are predicted by the formulae provided in Appendix A by setting arbitrary constants $C_0 = C_1 = D_{0\ldots3} = 0$, which leads to a transition from the general solution of non-homogeneous differential Equation (10) to the solution of homogeneous differential Equation (11).

In these plots, frequency ratio values $\mu_0 = 1.4 \times 10^{-3}$, $\mu_1 = 1.06 \times 10^{-2}$, and $\mu_2 = 2.51 \times 10^{-2}$ are calculated from the experimental data of the tested bridge over Susve's (Lithuania) river given in the next study. Also, the value of the static load-induced displacement $u_C^0 = 1.96$ mm is set for all cases considered. The vibration frequency of the vehicle suspension is taken as $f_V = 2.7$ Hz ($\omega_V = 16.97 \frac{1}{\mathrm{s}}$), and the free vibration frequency of the girder is $\omega_C = 26.1 \frac{1}{\mathrm{s}}$. The value of the imposed loading frequency equals $\theta = 2.69$ s^{-1} ($c = 20$ $\frac{\mathrm{m}}{\mathrm{s}}$). The value of parameter $k = 1$ and the frequencies is equal to $\lambda = 9.94$ and $\eta = 6.17$.

A convergence criterion for neglecting $O(\varepsilon^2)$ concerns the smallness values of the latter term. In particular, the magnitude of $\varepsilon = \mu_0$, since the best accuracy relative to the numerical solution is obtained by selecting k = 1. Hence, for $\mu_0 = 1.4 \times 10^{-3}$, $\varepsilon = 1.4 \times 10^{-3}$, which yields a negligible error on the order $\times 10^{-4}$% when omitting $O(\varepsilon^2)$ from the applied perturbation series.

Figure 2 demonstrates the interaction of girder–vehicle and vehicle–girder free vibrations. As can be seen from these plots, the motions are stable (i.e., bounded) for the girder and the suspension. In Figure 2a,b, despite the initial values of the vehicle suspension

$w(0) = w'(0) = 0$, the applied initial excitation via non-dimensional displacement of the girder $u(0) \neq 0$ or its rate $u'(0) \neq 0$ sets in motion vertical vibrations of the suspension. This implies that in the case of the free vibrations of the girder due to $u(0) \neq 0$ or $u'(0) \neq 0$, the vehicle suspension also starts vibrating vertically due to the girder–vehicle interaction, i.e., suspension transmissibility factor $w(\xi) \neq 0$. Similarly, in Figure 2c,d, the vehicle–girder interaction is specified by applying the initial excitation subjected to $w(0) \neq 0$ or $w'(0) \neq 0$, which further results in $u(\xi) \neq 0$, despite the initial conditions of a rest state of the girder being provided for $u(0) = 0$ or $u'(0) = 0$. All these interactions are possible, if $\mu_0 \neq 0$; otherwise, the girder and vehicle suspension vibrations are independent (no interaction). Moreover, as the mass of the girder significantly exceeds the mass of the vehicle, the amplitude of the free vibrations of the bridge girder increases very slowly with time. When four fundamental non-dimensional functions $u(t)$ and four non-dimensional fundamental functions $w(t)$ are given in terms of the set of the initial conditions of the unit (22), the solution of the homogeneous system of Equation (11) can be rescaled to the free vibrations of the real interaction between the girder and the suspension via the multiplication of functions $u(\xi)$ and $w(\xi)$ (Figure 2) by the real values of displacements or velocities imposed. In Figure 2, frequency ratios μ are taken from the experimental tests.

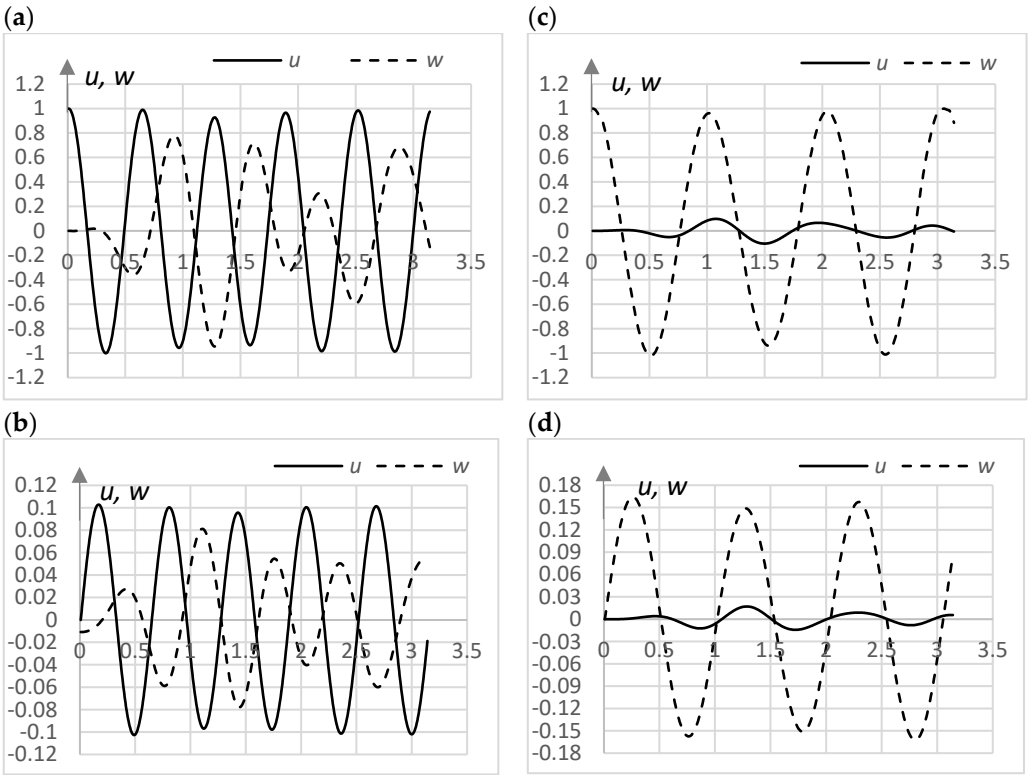


Figure 2. Fundamental solutions for the set of homogeneous differential equations for the interaction between the girder (regular lines) and the vehicle suspension (dashed lines), when the initial conditions are (**a**) $u(0) = 1$, $u'(0) = 0$, $w(0) = w'(0) = 0$, (**b**) $u'(0) = 1$, $u(0) = 0$, $w(0) = w'(0) = 0$, (**c**) $u(0) = u'(0) = 0$, $w(0) = 1$, $w'(0) = 0$, and (**d**) $u(0) = u'(0) = 0$, $w(0) = 0$, $w'(0) = 1$.

The derived equations are valid for $0 \leq \xi \leq \pi$; otherwise, the vehicle passes the girder, and the free vibrations of the girder and the vehicle can be represented classically via harmonic functions by setting the initial values of these functions as being equal to those at the end of the girder–vehicle interaction, when $\xi = \pi$.

Finally, the solutions in Equations (18)–(20) satisfy the equations in set (11), if the value of the girder–vehicle interaction frequency ratio $\mu_0 = \theta^2 \frac{m_V}{k_C} = \mu_1 \frac{m_V}{m_C}$ is small. Since $m_C \gg m_V$ is valid for most bridges and vehicles, the formulae derived are of sufficient

practical applicability. When μ_0 increases, the applied approximations (12 and 13) result in an instability of the mechanical system. In this case, stability regions in μ_0, μ_1, and μ_2 spaces should be determined in the same way as the stability charts of the Mathieu differential equation [22]. Meanwhile, for more rigorous mathematical analysis, Heun's local function can be considered.

4.2. A System of Non-Homogeneous Equations

Finally, the general solution for the set of non-homogeneous Equation (10) can be derived. In this case, the general solution for the set of non-homogeneous equations combines any (non-trivial) *particular* solution of the set of non-homogeneous differential equations with the *general* solution of the set of homogeneous differential equations. The latter solution is given above, while the particular solution of non-homogeneous equations is yet to be given. To this end, unknowns u and w in the particular solution for non-homogeneous equations will be denoted by U and W, respectively.

By applying Equations (12) and (13) in the non-homogeneous differential Equation (10), we can represent the first approximation of the solution as follows:

$$\begin{cases} q_{10}U_0'' + p_{10}U_0 = sin\xi, \\ q_{20}W_0'' + p_{20}W_0 = U_0 sin\xi \end{cases} \tag{23}$$

Meanwhile, the second approximation of the solution is the following:

$$\begin{cases} q_{10}U_1'' + p_{10}U_1 = -kW_0'' sin\xi - q_{11}U_0'' - p_{11}U_0, \\ q_{20}W_1'' + p_{20}W_1 = U_1 sin\xi - q_{21}W_0'' - p_{21}W_0. \end{cases} \tag{24}$$

Straightforwardly, a particular solution of system (23) can be represented using the following set:

$$\begin{cases} U_0 = 2C_0 cos\xi, \\ W_0 = \frac{C_0}{q_{20}}\left(\frac{1}{\eta^2} - \frac{cos2\xi}{\eta^2-4}\right), \end{cases} \tag{25}$$

where $C_0 = \frac{1}{2q_{10}(\lambda^2-1)}$.

By applying these expressions in the first equation of set (24), we obtain U_1, and then we get W_1 from the second equation of the set:

$$\begin{cases} U_1 = 2C_0D_0 sin\xi - 2C_1D_1 sin3\xi, \\ W_1 = \frac{D_2}{p_{20}} + \frac{D_3 cos2\xi}{q_{20}(\eta^2-4)} + \frac{C_1D_1 cos4\xi}{q_{20}(\eta^2-16)}, \end{cases} \tag{26}$$

where $C_1 = \frac{1}{2q_{10}(\lambda^2-9)}$, $D_0 = D_1 + 2C_0(q_{11} - p_{11})$, $D_1 = \frac{2kC_0}{q_{20}(\eta^2-4)}$, $D_2 = C_0\left(D_0 - \frac{p_{21}}{q_{20}\eta^2}\right)$, and $D_3 = \frac{C_0}{q_{20}}\frac{p_{21}-4q_{21}}{\eta^2-4} - C_0D_0 - C_1D_1$.

Finally, the general solution for the set of non-homogeneous Equation (10) provides the sum of the particular solutions (25) and (26), plus the general solution for homogeneous Equation (13), where U_0, W_0, U_1, and W_1 are in Equations (18)–(20). Thus:

$$\begin{cases} u(\xi) = u_0 + \varepsilon u_1 + U_0 + \varepsilon U_1, \\ w(\xi) = w_0 + \varepsilon w_1 + W_0 + \varepsilon W_1. \end{cases} \tag{27}$$

The general solution of the non-homogeneous Equation (27) has arbitrary constants A_1, A_2, B_1, B_2 and A_3, A_4 and B_3, B_4, coming from the general solution of the set of homogeneous equations, which require the solution of eight linear equations with eight unknowns to fulfill the initial values of the bridge–vehicle response. Thus, for the simplest cases of interaction, only six initial values of the dynamic variables ranging from the displacements

up to the accelerations for the girder and the suspension could be set. As a result, the prediction of arbitrary constants provides the iterative process.

In particular, let us assume the initial values of the non-dimensional displacement of the girder to be equal to $u(0) \equiv u_n$, and its rate to be given as $u'(0) \equiv u_v$; similarly, $w(0) \equiv w_n$ and $w'(0) \equiv w_v$ are imposed for the vertical motion of the suspension. Let the initial values be also decomposed using two approximations by the following set:

$$\begin{cases} \begin{cases} u_n = u_{n0} + \varepsilon u_{n1} \\ w_n = w_{n0} + \varepsilon w_{n1} \end{cases}, \\ \begin{cases} u_v = u_{v0} + \varepsilon u_{v1} \\ w_v = w_{v0} + \varepsilon w_{v1} \end{cases}. \end{cases} \tag{28}$$

where u_{n0}, w_{n0}, u_{v0}, w_{v0} and U_{n1}, W_{n1}, U_{v1}, W_{v1} are the initial values for the girder and the vehicle suspension for the first and the second approximations, respectively.

Since the initial values are decomposed for the first and the second approximations, we have additional equations to get the required number of equations to find all arbitrary constants (Appendix A). Since only the initial values of the general solution of Equation (10) are known, the initial values for the approximations are selected arbitrarily and should be corrected subsequently to obtain the state of dynamic equilibrium with minimal errors in $\xi \in [0, \pi]$. Let us suppose that any initial values of the variables of the second approximation are set. Thus, using solutions (18) and (25) along with their rates, we arrive at four equations to find constants A_1, A_2, B_1 and B_2:

$$\begin{cases} u_{n0} = u_0(0) + U_0(0) \\ u_{v0} = u_0'(0) + U_0'(0) \\ w_{n0} = w_0(0) + W_0(0) \\ w_{v0} = w_0'(0) + W_0'(0) \end{cases} \tag{29}$$

where rates $u_0'(\xi)$, $U_0'(\xi)$, $w_0'(\xi)$, and $W_0'(\xi)$ are simply found analytically from (18) and (25) and by taking their initial values for $\xi = 0$.

Next, we can find constants A_3, A_4 and B_3, B_4 by applying the corrected solutions of the dynamic variables using Equations (19) and (26):

$$\begin{cases} u_{n1} = u_1(0) + U_1(0) \\ u_{v1} = u_1'(0) + U_1'(0) \\ w_{n1} = w_1(0) + W_1(0) \\ w_{v1} = w_1'(0) + W_1'(0) \end{cases} \tag{30}$$

The iterative process for predicting the arbitrary constants to satisfy the initial values of the dynamic variables can be satisfactorily ended by applying a *dynamic* equilibrium condition. Its criterion for the best match of the initial values can be written from Equation (10), as follows:

$$\begin{cases} \delta_1(\xi) = \mu_1 u'' + u - sin\xi(1 - \mu_0 w'') \\ \delta_2(\xi) = \mu_2 w'' + w - usin\xi \end{cases} \tag{31}$$

Thus, for $\delta_1(\xi) = \delta_2(\xi) \equiv 0$, the dynamic equilibrium conditions in the bridge–girder interaction are completely satisfied, fulfilling the set of motion Equation (10). Otherwise, the relative mean square errors

$$\begin{cases} \varepsilon_u^2 = \int_0^\pi \delta_1^2 d\xi \Big/ \int_0^\pi u^2 d\xi \\ \varepsilon_w^2 = \int_0^\pi \delta_2^2 d\xi \Big/ \int_0^\pi w^2 d\xi \end{cases}, \tag{32}$$

are required to be minimized by correcting the selected values of the arbitrary constant in the next iteration.

In general, different criteria (e.g., energy balance, among others) can be applied in predicting the arbitrary constants. In fact, the zero-value-based initial values of dynamic variables $u(0) = u'(0) = u''(0)$ and $w(0) = w'(0) = w''(0)$ are of practical use in most situations of bridge testing and monitoring. In this case, if the initial values for the second approximation are $u_{n1} = u_{v1} = w_{n1} = w_{v1} = 0$, then initial values u_n, w_n, u_v, and w_v are also the same.

The derived formulae for the prediction of arbitrary constants $A_{1\ldots4}$ and $B_{1\ldots4}$ are given in Appendix A for the initial values of the first and the second approximations.

5. Results of Approximate Analytical and Numerical Solutions

The proposed approximate analytical solution of the dynamic equations provides the final version of the formulae in the real domain of the variables. The formulae derived will hereinafter be directly applied to the dynamic analysis of the bridge–girder response. The presented formulae were given mostly omitting the details of the mathematical re-arrangements, since they are not in the closed form. Moreover, the presented derivation was initially conducted in the complex plane of variables and an arbitrary constant, which also provides the verification of the solution. Meanwhile, the solution technique was implemented in a simple code written using Matlab software.

In Figure 3, the approximate analytical girder–suspension response is calculated by the general solution of (27) along with the numerical solution of Equation (3) via the implemented 5th order Gear predictor–corrector time integration technique given in Appendix A. In these plots, the results of the approximate analytical prediction are denoted using the subscript (*th*). All initial values of the dynamic variables are set to zero. The transition from the non-dimensional variables to girder mid-span and vehicle suspension displacements are given as $u_C(t) = u(\theta t)u_C^0$, $w_V(t) = w(\theta t)u_C^0$, where the value of static load-induced displacement $u_C^0 = 1.96$ mm is set for all the cases considered. The data on the girder and the vehicle are taken from the bridge experimental investigation. Here, the vehicle suspension vibration frequency is taken as $f_V = 2.7$ Hz ($\omega_V = 16.97\frac{1}{\mathrm{s}}$), while the girder's free vibration frequency is $\omega_C = 26.06\frac{1}{\mathrm{s}}$. The values of the imposed loading frequencies are $\theta = 0.67\ \mathrm{s}^{-1}$ ($c = 5\frac{\mathrm{m}}{\mathrm{s}}$ and $\theta = 4.03\ \mathrm{s}^{-1}$ ($c = 30\frac{\mathrm{m}}{\mathrm{s}}$). The value of parameter $k = 1$ is used during the approximate analytical prediction.

As can be seen in Figure 3, when using Equation (27), the approximate analytically predicted girder mid-span displacements are fairly coincident with those computed numerically. The same accuracy is also observed in the case of vehicle motion speed. The time evolution of the analytically predicted vertical displacement of vehicle suspension as well as its rate exhibit a small increase in the prediction errors for the case of slow vehicle motion (cf. a,b and c,d in Figure 3).

As can be seen in Figure 3, completely different bridge–vehicle dynamic behavior occurs, when the dynamic action results from slow ($c = 5$ m/s (18 km/h)) and rapid ($c = 30$ m/s (108 km/h)) vehicle motion over the girder (cf. a–c and d–f in Figure 3). In particular, slow vehicle motion generates small and frequent fluctuations in the evolution of girder mid-span displacement, while the maxima, $\max(u_C(t)) \approx 2$ mm, of the function of girder mid-span displacement remain near the value of static displacement, $u_C^0 = 1.96$ mm, due to load G_V. Dynamic factor $D_u = \max(u_C(t))/u_C^0 = 1.015$ results in a negligible dynamic effect for the girder and the suspension considered. On the contrary, in the case of rapid motion of the vehicle, the evolution of small vibrations in the $u_C(t)$ function transforms into the development of a finite number of fluctuations. The fluctuations evolve towards the direction of the motion of the vehicle and result in an increase in the maximal values of displacements of the girder and the vehicle. As a result, the dynamic factor of the

girder displacement increases to $D_u = \max(u_C(t))/u_C^0 = 1.19$, which leads to a significant dynamic effect for the selected properties of the girder and the suspension.

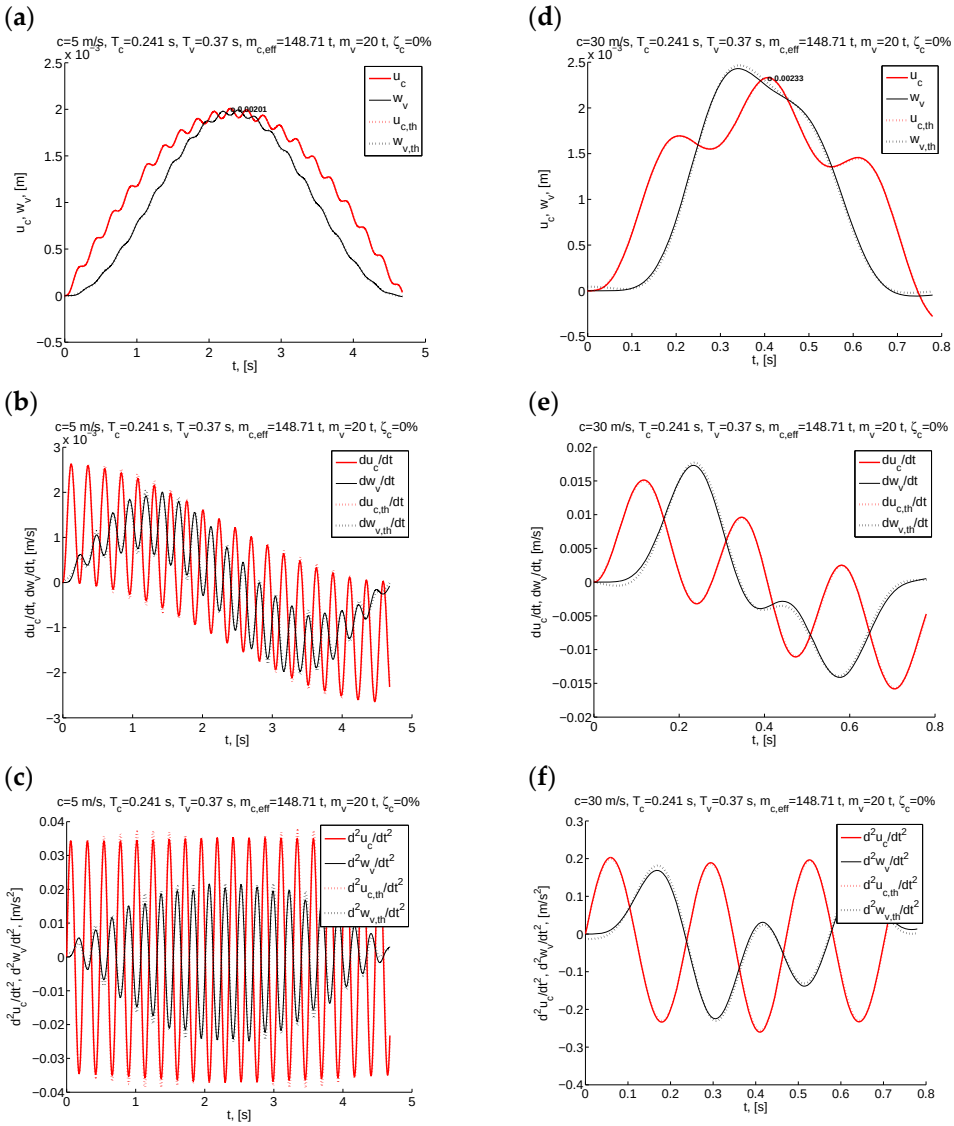


Figure 3. Evolution of bridge girder mid-span and vehicle suspension vertical displacements, along with their velocities and accelerations, without viscous damping: (**a**–**c**) vehicle speed c = 18 km/h; (**d**–**f**) c = 108 km/h.

The dynamic effects are subjected to a competitive evolution of the inertial force, $\Phi_V(t)$, of the suspension, which generates a diminishing effect on $u_C(t)$, while the evolution of the dynamic displacement, $w_V(t)$, of the suspension leads to an increase in the values of girder mid-span displacement.

Energy dissipation of various origin takes place in bridge girders. The approximate analytical solution is found when the viscous-damping force (Figure 1) is set to zero. For practical purposes, it is reasonable to consider the effect of viscous damping on the dynamic response of the bridge girder. To this end, Figure 4 demonstrates the effect of ζ_C = 5% viscous damping on the evolution of the dynamic variables of the girder and the vehicle suspension. The case of damped vibrations is resolved numerically (cf. Appendix B), while the undamped dynamic response is computed by Equation (27) and denoted in the plots with the subscript (*th*).

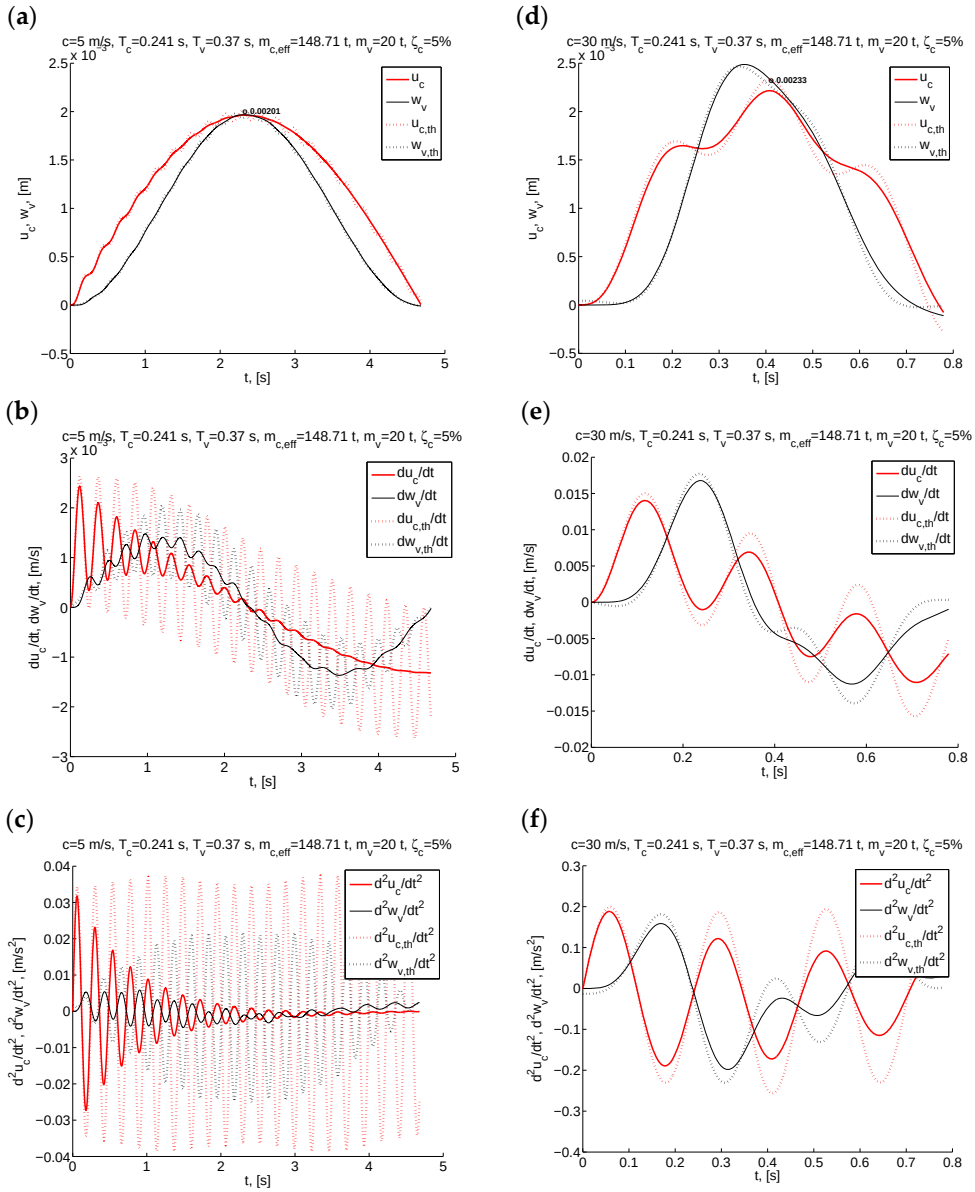


Figure 4. Evolution of bridge girder mid-span and vehicle suspension vertical displacements, along with their velocities and accelerations, with 5% viscous damping: (**a**–**c**) vehicle speed c = 18 km/h; (**d**–**f**) c = 108 km/h.

As can be seen in Figure 4, 5% viscous damping of the girder, which is mostly suited to reinforced concrete structures, has a mild effect on its mid-span displacement (Figure 4a,c). In particular, the small displacement oscillations caused by slow motion (c = 18 km/h) of the vehicle over the girder are completely damped (Figure 4a), and the maximal value of displacement lies essentially at the values induced by static loading. For rapid motion of the vehicle, the damping effect evolves similarly, while the decrease in the displacement maxi is sufficiently small (Figure 4c). As is expected, viscous damping affects bridge and vehicle suspension displacement rates (Figure 4b,d). Thus, in the case of 5% viscous damping of the girder, the obtained results show a mild effect on the evolution of the vertical displacements of girder mid-span and vehicle suspension, showcasing the ability for approximate analytical prediction by applying the derived formulas. In cases where the effect of damping could be sufficient, the numerical model is applicable instead.

The errors of the proposed analytical solution are given in Table 1. In this case, 95% confidence intervals of the relative errors are calculated for the degree of freedom of the more than 600 samples, considering the selected dynamic parameters.

Table 1. Ninety-five percent confidence intervals of the relative errors of the analytical method and dynamic parameters.

	m_v = *20,000* kg	*Tc* = *0.24* s	*Tv* = *0.37* s	f_v = *2.7* Hz	
	c = 5 m/s	c = 10 m/s	c = 20 m/s	c = 30 m/s	c = 40 m/s
Error, %	[2.01, 2.09]	[2.06, 2.15]	[2.26, 2.40]	[2.29, 2.45]	[4.51, 5.26]
η	24.928	12.409	6.2	4.127	3.072
λ	39.56	19.865	9.937	6.631	5.003
$\omega_c + \theta$, 1/*s*	51.123	38.604	32.394	30.322	29.267
ω_v, 1/*s*			16.965		
$\mu_0 = \varepsilon$	8.832×10^{-5}	3.533×10^{-4}	1.413×10^{-3}	3.180×10^{-3}	5.653×10^{-3}
μ_1	6.567×10^{-4}	2.627×10^{-3}	1.051×10^{-2}	2.364×10^{-2}	4.203×10^{-2}
μ_2	1.566×10^{-3}	6.263×10^{-3}	2.505×10^{-2}	5.637×10^{-2}	1.002×10^{-1}
	m_v = *40,000* kg	*Tc* = *0.17* s	*Tv* = *0.37* s	f_v = *2.7* Hz	
	c = 5 m/s	c = 10 m/s	c = 20 m/s	c = 30 m/s	c = 40 m/s
Error, %	[1.71, 1.74]	[1.73, 1.77]	[1.74, 1.81]	[1.72, 1.84]	[2.72, 2.98]
η	24.847	12.423	6.211	4.139	3.103
λ	56.129	28.065	14.033	9.356	7.018
ω_c+θ, 1/*s*	61.892	49.468	43.255	41.184	40.148
ω_v, 1/*s*			16.965		
$\mu_0 = \varepsilon$	8.832×10^{-5}	3.533×10^{-4}	1.413×10^{-3}	3.180×10^{-3}	5.653×10^{-3}
μ_1	3.284×10^{-4}	1.313×10^{-3}	5.254×10^{-3}	1.182×10^{-2}	2.102×10^{-2}
μ_2	1.566×10^{-3}	6.263×10^{-3}	2.505×10^{-2}	5.637×10^{-2}	1.002×10^{-1}
	m_v = *20,000* kg	*Tc* = *0.339* s	*Tv* = *0.37* s	f_v = *2.7* Hz	
	c = 5 m/s	c = 10 m/s	c = 20 m/s	c = 30 m/s	c = 40 m/s
Error, %	[3.95, 4.15]	[4.83, 5.11]	[5.01, 5.61]	[4.70, 5.28]	[5.61, 6.91]
η	24.665	12.103	6.888	4.4486	3.1996
λ	28.265	14.386	7.0675	4.7016	3.4884
$\omega_c + \theta$, 1/*s*	43.188	30.626	25.411	22.971	21.722
ω_v, 1/*s*			16.965		
$\mu_0 = \varepsilon$	8.832×10^{-5}	3.533×10^{-4}	1.413×10^{-3}	3.180×10^{-3}	5.653×10^{-3}
μ_1	1.313×10^{-3}	5.254×10^{-3}	2.102×10^{-2}	4.728×10^{-2}	8.406×10^{-2}
μ_2	1.566×10^{-3}	6.263×10^{-3}	2.505×10^{-2}	5.637×10^{-2}	1.002×10^{-1}
	m_v = *40,000* kg	*Tc* = *0.24* s	*Tv* = *0.37* s	f_v = *2.7* Hz	
	c = 5 m/s	c = 10 m/s	c = 20 m/s	c = 30 m/s	c = 40 m/s
Error, %	[2.03, 2.09]	[2.06, 2.15]	[2.26, 2.40]	[2.28, 2.46]	[4.51, 5.24]
η	24.823	12.409	6.2	4.127	3.070
λ	39.726	19.865	9.937	6.631	5.000
$\omega_c + \theta$, 1/*s*	51.018	38.604	32.394	30.322	29.264
ω_v, 1/*s*			16.965		

Table 1. *Cont.*

$\mu_0 = \varepsilon$	8.832×10^{-5}	3.533×10^{-4}	1.413×10^{-3}	3.180×10^{-3}	5.653×10^{-3}
μ_1	6.567×10^{-4}	2.627×10^{-3}	1.051×10^{-2}	2.364×10^{-2}	4.203×10^{-2}
μ_2	1.566×10^{-3}	6.263×10^{-3}	2.505×10^{-2}	5.637×10^{-2}	1.002×10^{-1}
	$m_v = 20{,}000$ kg	$Tc = 0.415$ s	$Tv = 0.37$ s	$f_v = 2.7$ Hz	
	$c = 5$ m/s	$c = 10$ m/s	$c = 20$ m/s	$c = 30$ m/s	$c = 40$ m/s
Error, %	[3.59, 3.74]	[4.38, 4.71]	[5.76, 6.74]	[5.33, 6.50]	[8.47, 12.72]
η	26.184	13.00	6.24	4.186	3.146
λ	21.736	10.931	5.723	3.791	2.836
$\omega_c + \theta$, 1/s	41.308	28.128	21.364	19.309	18.27
ω_v, 1/s			16.965		
$\mu_0 = \varepsilon$	8.832×10^{-5}	3.533×10^{-4}	1.413×10^{-3}	3.180×10^{-3}	5.653×10^{-3}
μ_1	1.970×10^{-4}	7.881×10^{-3}	3.152×10^{-2}	7.093×10^{-2}	1.261×10^{-1}
μ_2	1.566×10^{-3}	6.263×10^{-3}	2.505×10^{-2}	5.637×10^{-2}	1.002×10^{-1}
	$m_v = 40{,}000$ kg	$Tc = 0.294$ s	$Tv = 0.37$ s	$f_v = 2.7$ Hz	
	$c = 5$ m/s	$c = 10$ m/s	$c = 20$ m/s	$c = 30$ m/s	$c = 40$ m/s
Error, %	[2.91, 3.06]	[3.09, 3.32]	[3.84, 4.09]	[4.88, 5.32]	[6.49, 7.58]
η	24.926	12.455	6.095	4.023	3.242
λ	32.302	16.159	8.242	5.531	3.923
$\omega_c + \theta$, 1/s	46.314	33.828	27.483	25.411	24.630
ω_v, 1/s			16.965		
$\mu_0 = \varepsilon$	8.832×10^{-5}	3.533×10^{-4}	1.413×10^{-3}	3.180×10^{-3}	5.653×10^{-3}
μ_1	9.851×10^{-4}	3.940×10^{-3}	1.576×10^{-2}	3.546×10^{-2}	6.305×10^{-2}
μ_2	1.566×10^{-3}	6.263×10^{-3}	2.505×10^{-2}	5.637×10^{-2}	1.002×10^{-1}
	$m_v = 20{,}000$ kg	$Tc = 0.24$ s	$Tv = 0.185$ s	$f_v = 5.4$ Hz	
	$c = 5$ m/s	$c = 10$ m/s	$c = 20$ m/s	$c = 30$ m/s	$c = 40$ m/s
Error, %	[3.57, 3.71]	[4.85, 5.15]	[5.92, 6.30]	[6.33, 6.89]	[8.20, 9.01]
η	51.951	25.986	13.412	8.973	6.763
λ	37.963	18.97	9.173	6.078	4.159
$\omega_c + \theta$, 1/s	78.145	52.181	39.607	35.168	32.958
ω_v, 1/s			33.929		
$\mu_0 = \varepsilon$	8.832×10^{-5}	3.533×10^{-4}	1.413×10^{-3}	3.180×10^{-3}	5.653×10^{-3}
μ_1	6.567×10^{-4}	2.627×10^{-3}	1.051×10^{-2}	2.364×10^{-2}	4.203×10^{-2}
μ_2	3.914×10^{-4}	1.566×10^{-3}	6.263×10^{-3}	1.409×10^{-2}	2.505×10^{-2}
	$m_v = 40{,}000$ kg	$Tc = 0.17$ s	$Tv = 0.185$ s	$f_v = 5.4$ Hz	
	$c = 5$ m/s	$c = 10$ m/s	$c = 20$ m/s	$c = 30$ m/s	$c = 40$ m/s
Error, %	[6.24, 6.30]	[6.20, 6.36]	[8.00, 8.51]	[11.06, 12.01]	[11.53, 12.56]
η	47.632	23.794	12.103	8.701	7.370
λ	58.555	29.293	14.386	9.023	7.520
$\omega_c + \theta$, 1/s	84.677	60.839	49.148	45.746	44.415
ω_v, 1/s			33.929		
$\mu_0 = \varepsilon$	8.832×10^{-5}	3.533×10^{-4}	1.413×10^{-3}	3.180×10^{-3}	5.653×10^{-3}
μ_1	3.284×10^{-4}	1.313×10^{-3}	5.254×10^{-3}	1.182×10^{-2}	2.102×10^{-2}

Table 1. *Cont.*

μ_2	3.914×10^{-4}	1.566×10^{-3}	6.263×10^{-3}	1.409×10^{-2}	2.505×10^{-2}
	$m_v = 20{,}000$ kg	$Tc = 0.339$ s	$Tv = 0.185$ s	$f_v = 5.4$ Hz	
	$c = 5$ m/s	$c = 10$ m/s	$c = 20$ m/s	$c = 30$ m/s	$c = 40$ m/s
Error, %	[2.11, 2.17]	[2.22, 2.31]	[2.22, 2.37]	[2.49, 2.74]	[3.20, 3.66]
η	51.676	25.841	12.928	8.627	6.479
λ	26.987	13.490	6.737	4.482	3.351
$\omega_c + \theta$, 1/s	70.198	44.364	31.450	27.149	25.001
ω_v, 1/s			33.929		
$\mu_0 = \varepsilon$	8.832×10^{-5}	3.533×10^{-4}	1.413×10^{-3}	3.180×10^{-3}	5.653×10^{-3}
μ_1	1.313×10^{-3}	5.254×10^{-3}	2.102×10^{-2}	4.728×10^{-2}	8.406×10^{-2}
μ_2	3.914×10^{-4}	1.566×10^{-3}	6.263×10^{-3}	1.409×10^{-2}	2.505×10^{-2}
	$m_v = 40{,}000$ kg	$Tc = 0.24$ s	$Tv = 0.185$ s	$f_v = 5.4$ Hz	
	$c = 5$ m/s	$c = 10$ m/s	$c = 20$ m/s	$c = 30$ m/s	$c = 40$ m/s
Error, %	[3.57, 3.71]	[4.85, 5.15]	[5.71, 6.13]	[6.33, 6.89]	[8.04, 8.90]
η	51.951	25.986	13.292	8.973	6.635
λ	37.963	18.970	9.258	6.078	4.616
$\omega_c + \theta$, 1/s	78.145	52.181	39.487	35.168	32.830
ω_v, 1/s			33.929		
$\mu_0 = \varepsilon$	8.832×10^{-5}	3.533×10^{-4}	1.413×10^{-3}	3.180×10^{-3}	5.653×10^{-3}
μ_1	6.567×10^{-4}	2.627×10^{-3}	1.051×10^{-2}	2.364×10^{-2}	4.203×10^{-2}
μ_2	3.914×10^{-4}	1.566×10^{-3}	6.263×10^{-3}	1.409×10^{-2}	2.505×10^{-2}
	$m_v = 20{,}000$ kg	$Tc = 0.415$ s	$Tv = 0.185$ s	$f_v = 5.4$ Hz	
	$c = 5$ m/s	$c = 10$ m/s	$c = 20$ m/s	$c = 30$ m/s	$c = 40$ m/s
Error, %	[1.31, 1.35]	[1.37, 1.44]	[1.18, 1.29]	[1.81, 2.05]	[2.98, 6.2]
η	51.229	25.616	12.812	8.545	6.484
λ	22.227	11.112	5.552	3.696	2.731
$\omega_c + \theta$, 1/s	66.352	40.74	27.935	23.669	21.608
ω_v, 1/s			33.929		
$\mu_0 = \varepsilon$	8.832×10^{-5}	3.533×10^{-4}	1.413×10^{-3}	3.180×10^{-3}	5.653×10^{-3}
μ_1	1.970×10^{-3}	7.881×10^{-3}	3.152×10^{-3}	7.093×10^{-2}	1.261×10^{-1}
μ_2	3.914×10^{-4}	1.566×10^{-3}	6.263×10^{-3}	1.409×10^{-2}	2.505×10^{-2}
	$m_v = 40{,}000$ kg	$Tc = 0.294$ s	$Tv = 0.185$ s	$f_v = 5.4$ Hz	
	$c = 5$ m/s	$c = 10$ m/s	$c = 20$ m/s	$c = 30$ m/s	$c = 40$ m/s
Error, %	[3.16, 3.24]	[3.26, 3.38]	[3.02, 3.23]	[3.34, 3.63]	[4.87, 5.43]
η	52.204	26.108	13.067	8.725	6.673
λ	30.846	15.416	7.694	5.113	3.744
$\omega_c + \theta$, 1/s	73.592	47.496	34.454	30.113	28.061
ω_v, 1/s			33.929		
$\mu_0 = \varepsilon$	8.832×10^{-5}	3.533×10^{-4}	1.413×10^{-3}	3.180×10^{-3}	5.653×10^{-3}
μ_1	9.851×10^{-4}	3.940×10^{-3}	1.576×10^{-2}	3.645×10^{-2}	6.305×10^{-2}
μ_2	3.914×10^{-4}	1.566×10^{-3}	6.263×10^{-3}	1.409×10^{-2}	2.505×10^{-2}

As shown in Table 1, in the majority of dynamical analysis cases, 95% confidence intervals for the relative errors of the approximate analytical solutions using Equation (27) range within 2–3%/. In general, this represents a highly accurate prediction for the first-order perturbation method applied to solving the coupled dynamic equations. It suggests that the mean error of the solution population within interval $t \in [0, t_u]$ falls within this 2–3% range with a 95% probability across the analyzed dynamic parameter scenarios. However, in cases where frequencies closely approach one another, i.e., when $\omega_C + \theta \leftrightarrow \omega_V$ and $\lambda \leftrightarrow \eta$, relative errors can increase up to 8–12% (Table 1). The details of this increment are analyzed below in Figure 5, where the accuracy of the approximate analytical prediction is examined for different cases of natural and loading frequencies. Different frequencies of the girder are defined by changing the mass of the girder and holding static mid-span displacement constant at $u_C^0 = 1.96$ mm.

As can be seen in Figure 5a,b, the approximate analytically predicted values of girder mid-span and vehicle suspension vertical displacements agree very well with those computed numerically. These plots refer to cases where the values of girder and loading frequencies *overestimate* the natural frequency of the suspension, i.e., $\omega_C + \theta = 65.4 > \omega_V = 34\frac{1}{s}$ for the slow motion of the vehicle (Figure 5a) and $\omega_C + \theta = 68.7 > \omega_V = 34\frac{1}{s}$ for its rapid motion over the bridge (Figure 5b). Similarly, in Figure 5e,f, a fairly accurate analytical prediction is given in the case where the girder and loading frequencies *underestimate* the natural frequency of the suspension, i.e., $\omega_C + \theta = 20.9 < \omega_V = 34\frac{1}{s}$ for the slow motion of the vehicle (Figure 5e) and $\omega_C + \theta = 24.2 < \omega_V = 34\frac{1}{s}$ for its rapid motion (Figure 5f). In the approximate analytical predictions, values $k = 1$ and $\varepsilon = \mu_0/k$ are simply set.

In general, the results of Equation (27) demonstrate a good compromise between the possibilities of an analytical solution and reasonable accuracy. However, when the total frequency of the girder and loading has the tendency to approach the suspension frequency or vice versa, i.e., $\omega_C + \theta \leftrightarrow \omega_V$ and $\lambda \leftrightarrow \eta$, the approximate analytical prediction results in an increase in errors compared to the results obtained with the numerical analysis (cf. Figure 5c,d). In particular, when $\omega_C + \theta = 32.7 \rightarrow \omega_V = 34\frac{1}{s}$ for the slow motion of the vehicle (Figure 5c) and $\omega_C + \theta = 36.1 \leftarrow \omega_V = 34\frac{1}{s}$ for the rapid motion (Figure 5d), the approximate analytically resolved $u_C(t)$, $w_V(t)$ functions highly deviate from those obtained numerically. Minimal deviations shown in Figure 5c,d are obtained when ε is set to 0, and the second approximation is not accounted for. In particular, errors (cf. Figure 5c,d) occur when $\lambda \leftrightarrow \eta$, since non-linear terms $O(\varepsilon^2)$ in power expansions (13) are neglected. Due to this, the multipliers $\frac{1}{\eta^2-(\lambda\pm1)^2}$ and $\frac{1}{\lambda^2-(\eta\pm1)^2}$ approach zero, resulting in a sufficient increase in the values of functions u_1 and w_1. They take place in the expressions of arbitrary constants A_3, A_4, and $B_{1\ldots4}$ and within terms $h_\pm$ and $h_\pm^*$ (cf. Appendix A).

For the limit cases, when $\eta^2 = (\lambda \pm 1)^2$ or $\lambda^2 = (\eta \pm 1)^2$ and $\eta^2 = (\lambda \pm 3)^2$, the solutions can be singular or undefined, depending on zero values of the appropriate initial conditions. When undefined, the values of $h_\pm$, $h_\pm^*$, $s_\pm$, and some arbitrary constants are taken from limits $\eta^2 \rightarrow (\lambda \pm 1)^2$ or $\lambda^2 \rightarrow (\eta \pm 1)^2$ applying the L'Hôpital rule. Meanwhile, in assumed range $-4 < \eta - \lambda < 4$, we can set $\varepsilon = 0$ to avoid an excessive increase in function w_1 values and to reduce the error of the approximate analytical solution (Figure 5d) in comparison with the exact (numerical) prediction.

On the other hand, at best, the key findings in the solutions of Mathieu's equation tend to only exist in numerical tables [18] composed of infinite continued fraction methods or approximate expressions for eigenvalue calculations represented by stability charts. Recently, charts and analysis of ε functions for some selected mechanical problems were presented in [22].

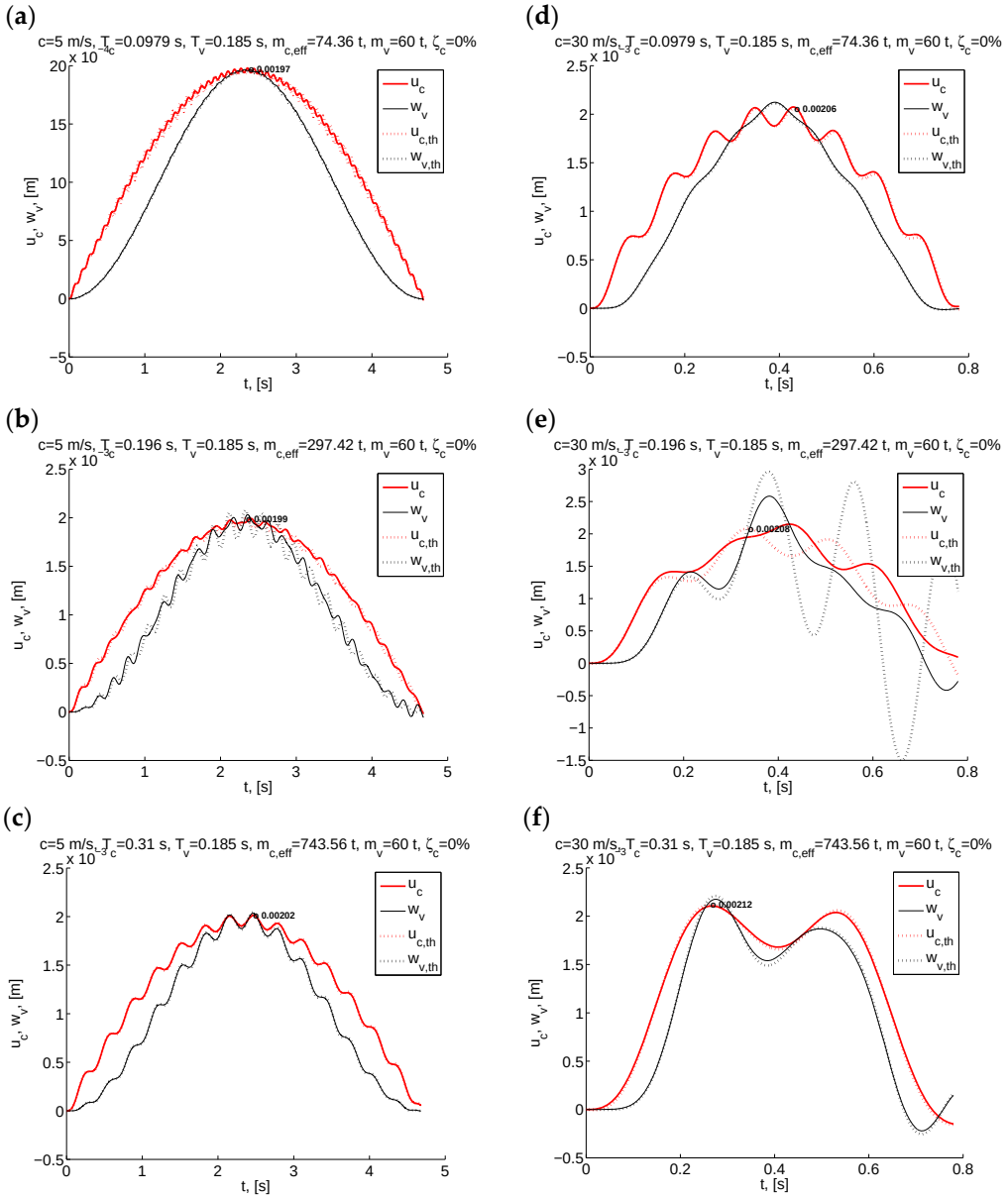


Figure 5. Evolution of bridge girder mid-span and vehicle suspension vertical displacements for different cases of girder, vehicle, and loading frequencies ω_c, ω_V: (**a**,**b**) $\omega_C + \theta > \omega_V$; (**c**,**d**) $\omega_C + \theta \leftrightarrow \omega_V$; (**e**,**f**) $\omega_C + \theta < \omega_V$.

On the basis of the obtained results, the range of the approximate analytical prediction can be summarized as follows:

1. A simply supported, relatively stiff girder undergoing first-mode kinematics, such as a *reinforced concrete* girder, provided for $m_C > m_V$, $k_C > k_V$;
2. Two-axle vehicle for a single-degree vibrating suspension approximation;
3. Combination of frequencies, such as $\omega_C + \theta \nrightarrow \omega_V$ and $\lambda \nrightarrow \eta$;
4. A smooth road surface, such as pavement of class A according to ISO 8608 providing for minimal roughness (not suited for class B).

Notably, no analytical damping provides a slightly conservative prediction for serviceability limit state design of reinforced concrete bridges possessing 5% regular damping.

As shown, the bridge and vibrating vehicle suspension interaction governs complex analytical prediction. However, simplified approximate relationships can also be considered below for appropriate cases of bridge–vehicle interaction.

6. Simplified Approximate Analytical Solutions of Differential Equations

From numerical analysis of dynamic Equation (2), for a sufficiently soft suspension, when $T_V \gg t_u = \frac{L}{c}$, the influence of the $w_V(t)$ function on mid-span displacement $u_C(t)$ delays resulting in a mild effect, and $u_C(t)$ is essentially subjected to the inertial force of the suspension $\Phi_V = -m_V \ddot{w}_V$. In particular, from Equation (2), we obtain $m_C \ddot{u}_C = -k_c u_C + k_V \left(\delta_0 + w_V \underbrace{-u_C \sin\theta t}_{\Phi_V/k_V,\, w_V=0} \right) \sin\theta t$. Thus, for $T_V \gg t_u$, we can imply that the inertial force of the vehicle suspension induces the main dynamical effect on the bridge mid-span displacement. Hence, in Equation (3), by setting $w_V = 0$, we obtain two separate dynamic equations, where the equation for girder mid-span displacement is defined as follows:

$$m_C \ddot{u}_C(t) + k_C u_C(t) \left(1 + \frac{k_V}{k_C} \sin^2 \theta t \right) = G_V \sin\theta t. \tag{33}$$

Thus, in this equation, girder spring stiffness constant $k_C \left(1 + \frac{k_V}{k_C} \sin^2 \theta t \right)$ is a time-varying parameter and depends on the loading frequency and the ratio of the suspension and girder constants. Meanwhile, this equation represents a Mathieu-type differential equation with a forcing term:

$$\mu_1 \ddot{u} + u \left(1 + \frac{\mu_0}{\mu_2} \sin^2 \xi \right) = \sin\xi. \tag{34}$$

The homogeneous component of Equation (34) can be represented in the standard canonical form of a Mathieu differential equation as follows:

$$\ddot{u} + (a - 2q\cos 2\xi\,)u = 0 \tag{35}$$

where $a = \frac{1}{\mu_1} + 2q$, $2q = \frac{\mu_0}{2\mu_2\mu_1}$, and parameter a is related, to some extent, to the natural frequency, while $2q$ provides for the parametric excitation amplitude in Equation (35).

The obtained equations are suitable for the analytical solution with respect to finding the simplified approximate formulae for mid-span displacement function $u_C(t)$. In this case, in Equations (14), (15), (23) and (24), we should set $p_{20} = p_{21} = 0$.

Since the simplification provided presumes applicability to soft suspensions with a long natural vibration period, i.e., $T_V \gg t_u$, it can also be expected that the bridge–vehicle interaction term is $1 + \frac{k_V}{k_C} \sin^2 \theta t \longrightarrow 1$, for $t \neq 0$, as $\frac{k_C}{k_V} \gg 1$, because girder stiffness usually overcomes vehicle suspension stiffness.

Thus, by setting $1 + \frac{k_V}{k_C} \sin^2 \theta t \approx 1$ in Equation (33), we can get the second simplified equation for an approximate prediction of the viscously damped girder mid-span displacement:

$$m_C \ddot{u}_C + k_C u_C + c_c \dot{u}_C = G_V \sin\theta t. \tag{36}$$

where c_c is the coefficient of viscous damping of the girder.

This is a linear non-homogeneous equation of the second order. The solution combines the general solution of a homogeneous differential equation (i.e., the response of a free-vibrating damped spring) with any particular solution of a non-homogeneous differential equation resulting from harmonic loading.

Thus, the homogeneous differential equation has the following solution:

$$u_{C,h}(t) = (A\cos\omega_D t + B\sin\omega_D t\,) e^{-\zeta_C \omega_C t}, \tag{37}$$

where A and B are arbitrary constants, $\omega_D = \omega_C\sqrt{1-\zeta_C^2}$ is the free vibration of the damped bridge girder, ζ_c is the girder damping ratio of a critical damping of a free-oscillating spring to a damping imposed, and $c_{crit} = 2m_C\omega_c$ is the girder's critical damping.

The particular solution of the non-homogeneous differential equation is

$$u_{C,nh}(t) = G_1\cos\theta t + G_2\sin\theta t, \tag{38}$$

where G_1 and G_2 are constants to satisfy the harmonic loading condition $G_V\sin\theta t$ in Equation (36). They are resolved from two equations rewritten in the matrix form:

$$\begin{bmatrix} 1-\mu_1 & 2\zeta_C\mu_1^{\frac{1}{2}} \\ -2\zeta_C\mu_1^{\frac{1}{2}} & 1-\mu_1 \end{bmatrix}\begin{Bmatrix} G_1 \\ G_2 \end{Bmatrix} = \begin{Bmatrix} 0 \\ u_C^0 \end{Bmatrix}. \tag{39}$$

As a result of the solution, the constants are calculated by applying the following formulae:

$$G_1 = u_C^0\frac{-2\zeta_C\mu_1^{\frac{1}{2}}}{(1-\mu_1)^2+4\zeta_C^2\mu_1}, \tag{40}$$

$$G_2 = u_C^0\frac{1-\mu_1}{(1-\mu_1)^2+4\zeta_C^2\mu_1}. \tag{41}$$

For initial conditions $u_C(0) = u'_C(0) = 0$, the arbitrary constants are simply defined from general solution $u_C(t) = u_{C,h}(t) + u_{C,nh}(t)$: $A = \frac{1}{\omega_D}\left(\zeta_C\omega_C B - \dot{u}_{C,nh}(0)\right)$, $B = -u_{C,nh}(0)$. Thus:

$$A = u_C^0\frac{2\zeta_C\mu_1^{\frac{1}{2}}}{(1-\mu_1)^2+4\zeta_C^2\mu_1} = -G_1, \tag{42}$$

$$B = u_C^0\frac{\omega_C\mu_1^{\frac{1}{2}}}{\omega_D}\frac{2\zeta_C^2-1+\mu_1}{(1-\mu_1)^2+4\zeta_C^2\mu_1}. \tag{43}$$

Finally, using the relationships of the arbitrary constants and the solutions of homogeneous and non-homogeneous differential equations, the general solution of Equation (11) is expressed as follows:

$$\begin{aligned} u_C(t) = \tfrac{u_C^0}{(1-\mu_1)^2+4\zeta_C^2\mu_1}\Big[\Big(\tfrac{\omega_C}{\omega_D}\left(2\zeta_C^2-1+\mu_1\right)\sin\omega_D t + 2\zeta_C\cos\omega_D t\Big) \\ \mu_1^{\frac{1}{2}}e^{-\zeta_C\omega_C t} + (1-\mu_1)\sin\theta t - 2\zeta_C\mu_1^{\frac{1}{2}}\cos\theta t\Big], \text{ for } T_V \gg t_u \text{ and } 1+\tfrac{k_V}{k_C}\sin^2\theta t \approx 1, \end{aligned} \tag{44}$$

The obtained formula fully neglects the bridge–vehicle interaction by setting $1+\frac{\mu_0}{\mu_2}\sin^2\xi \approx 1$, where $\frac{\mu_0}{\mu_2}$ is very small for the soft suspension, and provides the next analytical approximate relationship for predicting girder mid-span displacement.

A comparison of the results obtained by this formula with those calculated numerically accounting for girder–vehicle interaction is plotted in Figure 6. Predictions are given for the cases of soft (f_V = 0.5 Hz) and regular stiffness (f_V = 2.7 Hz) of the suspension.

As can be seen in Figure 6a,b, in the soft suspension case, the simplified approximate Equation (44) gives very accurate predictions when the dynamic effect on mid-span displacement is caused essentially by inertial force $\Phi_V(t)$ of the soft ($1+\frac{k_V}{k_C} = 1.002$) suspension. In the case of regular ($1+\frac{k_V}{k_C} = 1.06$) suspension stiffness, the approximate prediction results in prediction errors (Figure 6c,d). Approximate analytical prediction errors increase when the vehicle suspension becomes stiffer. The errors result from the bridge–vehicle interaction, when the dynamic effect on girder mid-span displacement is generated by the competitive interaction of the suspension's inertial force $\Phi_V(t)$ and its dynamic displace-

ment $w_V(t)$ (cf. Figure 6d). However, despite the errors of approximate prediction, the maxima of girder mid-span displacement are defined very accurately. Table 2 presents the relative errors of dynamic factor $D_u = \max u(t) \equiv \frac{\max u_C(t)}{u_C^0}$ prediction using Equation (44) vs. numerical prediction.

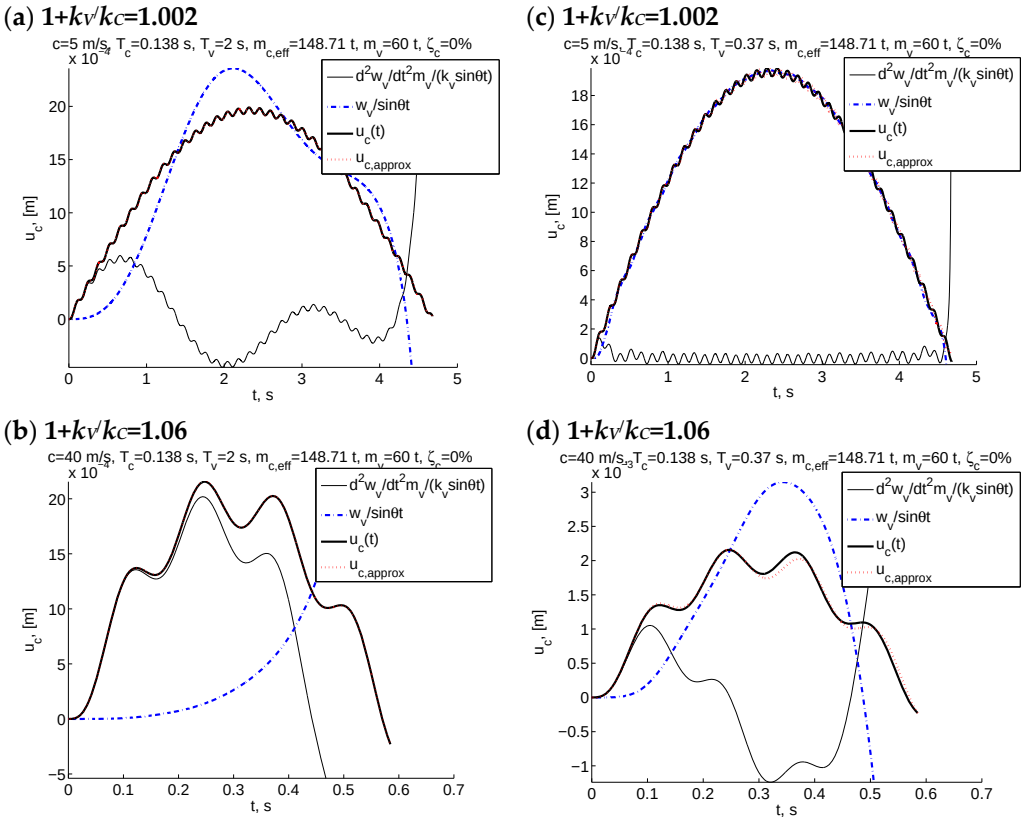


Figure 6. Evolution of girder mid-span displacement and the effect of the dynamic displacement of vehicle suspension and displacement due to the suspension's inertial force with respect to slow (**a**,**c**) and very rapid (**b**,**d**) vehicle motions. Cases of soft (f_V = 0.5 Hz) (a, b) and regular (f_V = 2.7 Hz) (**c**,**d**) suspension stiffness.

Table 2. Relative errors of the maximal values of the dynamic factor of mid-span displacement predicted using Equation (44) vs. the numerical solution.

T_C	$1 + k_V/k_C$	c = 10 m/s	c = 15 m/s	c = 20 m/s	c = 25 m/s	c = 30 m/s	c = 35 m/s	c = 40 m/s
0.095	1.003	−0.06%	0.05%	0.14%	0.09%	0.15%	0.12%	0.17%
0.117		−0.02%	0.04%	0.07%	0.13%	0.08%	0.17%	0.16%
0.165		−0.01%	0.08%	0.13%	0.08%	0.16%	0.15%	0.12%
0.234		−0.08%	0.03%	0.1%	0.16%	0.15%	0.12%	0.06%
0.286		−0.02%	0.11%	0.05%	0.15%	0.13%	0.07%	0.14%
	T_V/t_u	0.855	1.28	1.71	2.14	2.56	2.99	3.42

As can be seen from Table 2, the relative errors for the maximal values of dynamic factor $D_u = \max u(t) \equiv \frac{\max u_C(t)}{u_C^0}$ prediction using the approximate Equation (44) vs. numerical prediction are very small (not exceeding 0.2%) for the whole range of vehicle motion speed and natural vibration period of the girder. For the regular stiffness of the suspension (f_V = 2.7 Hz; measured experimentally during bridge testing over Susve's (Lithuania) river), when the bridge–vehicle dynamic interaction factor (i.e., the variable coefficient in the set of differential equations) is equal to $1 + \frac{k_V}{k_C}\sin^2\theta t = 1.06$ and its influence increases, the relative errors increase by up to 4%. In case of stiff suspension (f_V = 5.4 Hz,

$1 + \frac{k_V}{k_C} \sin^2 \theta t = 1.23$), the maximal error of the approximate prediction increases by up to 14%.

In cases where the total frequency of the girder and the loading has a tendency to approach the frequency of the suspension or vice versa, i.e., $\omega_C + \theta \leftrightarrow \omega_V$ (cf. Figure 5c,d), the results of $D_u = \max u(t)$ predicted by applying the approximate Equation (44) highly deviate from those computed numerically. In this case, the dynamic factor of girder mid-span displacement should be predicted either by an analytical solution using Equation (27) or numerically.

The maximal values of the dynamic factor $D_u = \max u(t)$ are of primary importance in serviceability limit state analysis of bridge design. Hence, it is worth analyzing these values analytically using the approximate Equation (44). In this case, the maximal values of the dynamic factor of girder mid-span displacement can be reached during resonance when $\mu_1 = 1$. Hence, from Equation (44), we can get:

$$u(t) = \frac{1}{2\zeta_C}\left[\left(\frac{\omega_C}{\omega_D}\zeta_C \sin\omega_D t + \cos\omega_D t\right)e^{-\zeta_C\omega_C t} - \cos\omega_C t\right], \text{ for} \mu_1 = 1. \tag{45}$$

From $\mu_1 = 1$, the resonance condition of the girder is simply provided for $t_u = \frac{1}{2}T_c$, which yields $t_u = \frac{\pi}{\omega_C}$. It also implies that resonance is defined by the forcing-frequency condition, while the transient amplitude develops during the finite vehicle-passage interval. At $t = t_u$, the vehicle passes the girder with speed $c_r = \frac{\omega_C L}{\pi}$, which provides a very high value for stiff girders (e.g., reinforced concrete bridges). By substituting $t = t_u$ in Equation (45), we can get the maximal value of the dynamic factor of mid-span displacement for a damped girder response:

$$D_{u,max} = \frac{1}{2\zeta_C}\left(1 - e^{-\pi\zeta_C}\right) \text{ for } \omega_C \approx \omega_D. \tag{46}$$

For $\zeta_C \in [0.05\ 0.1]$, there is $\omega_C \approx \omega_D$, and the range of the maximal values of the dynamic factor of girder mid-span displacement is $D_{u,max} \in \left[\frac{\pi}{2.16}\ \frac{\pi}{2.32}\right]$.

In the case of an undamped girder, where $\zeta_C = 0$, Equation (46) is undefined. We remove this uncertainty by applying L'Hôpital's rule and have:

$$D_{u,max} = \max u = \lim_{\zeta_C \to 0}\left(\frac{1}{2}\pi e^{-\pi\zeta_C}\right) = \frac{\pi}{2}. \text{ for } \zeta_C = 0. \tag{47}$$

Thus, in the case of an undamped girder, the maximal value of the dynamic factor of its mid-span displacement is $D_{u,max} = 1.57$. Indeed, these analytically determined values do not fully encompass the dynamic girder–suspension interaction and represent rather a theoretical approach to the limits of the dynamic factor for damped and undamped girders. On the other hand, in practice, there is a variety of sources for the dissipation of the imposed kinetic and stored energies, while the resonant effects are rarely available.

7. Conclusions

In the paper, the energetic Lagrangian approach has been applied to propose a two degrees-of-freedom lumped mass-spring-based model for prediction of the time-dependent evolution of girder mid-span and vehicle suspension vertical displacements, along with their rates and accelerations, subjected to the steady motion of the vehicle over the bridge on an ideally flat road surface. On the basis of the obtained results, the following conclusions have been drawn:

(1) Theoretically, it has been proven that the mid-span displacement of the girder results from the combined interaction of girder mid-span displacement, which is subjected to the inertial force of the moving vehicle suspension, and development of its dynamic displacement, which is also transferred to the girder mid-span.

(2) A general exact analytical solution for girder–vehicle dynamic equations does not exist, since two linear, non-homogeneous differential equations of the second order are governed by periodically variable coefficients. Moreover, the set of homogeneous differential equations provides two coupled differential Mathieu-type equations and theoretically governs a case of free vibration of the girder. Meanwhile, any excitation imposed either on the girder mid-span or on the suspension interacts with the moving weightless vehicle or vice versa. This effect is important when accounting for new developments in terms of cost-efficient bridge monitoring techniques, and when indirect identifications of bridge modal parameters are adopted via data recorded from sensors mounted directly on a moving vehicle.

(3) The proposed approximate analytical solution for girder–vehicle dynamic equations is governed by implementation of two sets of power series expansions and application of Lindstedt's singular perturbation method. This allowed for resolving of the algebraic equations for the girder mid-span displacement dynamic evolution factor and suspension transmissibility coefficient vs. dimensionless time, three ratios of the loading frequency with respect to the girder and the vehicle, and the combined interaction frequencies of free vibration.

(4) For the case of a soft suspension, when its natural vibration period is much longer than the time to pass the vehicle the girder, the vehicle suspension inertia force induces the main dynamic increase in the mid-span displacement, while the transfer of suspension dynamic displacement to the girder' mid-span is delayed. This effect is important allowing for separation of the dynamic interaction equations to attain a single homogeneous differential Mathieu's equation in its canonic form for the girder mid-span displacement. When the periodicity of this equation coefficient is negligible, the simplified approximate solution has been proposed.

(5) The approximate analytically predicted values of girder mid-span and vehicle suspension vertical displacements are of excellent agreement with those computed numerically in these cases, where the total values of girder and loading frequencies $\omega_C + \theta$ sufficiently overestimate or underestimate the frequency of vehicle suspension ω_V.

(6) When the total frequency of the girder and loading has the tendency to approach the suspension frequency or vice versa ($\omega_C + \theta \leftrightarrow \omega_V$ and $\lambda \leftrightarrow \eta$), the approximate analytical prediction deviates from the results of the numerical (exact) prediction. In this case, to minimize the error of the approximate analytical prediction proposed, factor k should be set to $k = 0$. For frequency case $\omega_C + \theta \leftrightarrow \omega_V$, a fairly accurate prediction is only feasible using numerical solutions (Appendix B).

Finally, the stability regions of the approximate analytical prediction remain to be further investigated in the space of the three principal frequency ratios (μ_0, μ_1, and μ_2) of the mechanical girder–suspension interaction system. In the next study, the verification of the model with respect to tests conducted on a real bridge girder is presented along with an evaluation of tractions exerted on the girder from the road surface roughness profile.

Author Contributions: Conceptualization, V.K.; methodology, M.A.; software, R.B.; validation, M.A. and R.B.; writing—original draft preparation, R.B. and M.A.; writing—review and editing, R.B.; supervision, V.K. All authors have read and agreed to the published version of the manuscript.

Funding: This research received no external funding.

Institutional Review Board Statement: Not applicable.

Informed Consent Statement: Not applicable.

Data Availability Statement: The data used in this study are available from the corresponding author upon reasonable request.

Conflicts of Interest: The authors declare no conflicts of interest.

Appendix A. Formulae and Prediction of Arbitrary Constants

A general solution of the set of non-homogeneous differential equations in Equation (10) yields the analytical solution by Equation (27), which involves arbitrary constants A_1, A_2 and B_1, B_2 coming from Equation (18) and A_3, A_4 and B_3, B_4 from Equation (20). They are calculated using the initial values according to Equation (28) and are as follows:

$$A_1 = \frac{1}{4}u_{n0};\ A_2 = \frac{u_{v0} - 2C_0}{4\lambda}; \tag{A1}$$

$$B_1 = \frac{E_1(u_{v0} - 2C_0)}{4q_{20}\lambda} + \frac{1}{4}w_{n0} + \frac{C_0}{q_{20}\eta^2(\eta^2 - 4)};\ B_2 = \frac{w_{v0}}{4\eta} - \frac{u_{n0}E_2}{4\eta q_{20}}; \tag{A2}$$

$$\text{where } E_1 = \frac{1}{2}\left(\frac{1}{P_{1p}} - \frac{1}{P_{1m}}\right);\ E_2 = \frac{1}{2}\left(\frac{\lambda+1}{P_{1p}} - \frac{\lambda-1}{P_{1m}}\right), \text{for } P_{1p} \neq 0, P_{1m} \neq 0. \tag{A3}$$

$$P_{1+} = P_{1p} = \eta^2 - (\lambda+1)^2;\ P_{1-} = P_{1m} = \eta^2 - (\lambda-1)^2; \tag{A4}$$

$$A_3 = \frac{1}{2}u_{n1} - A_1(h_p - h_m) - B_2(h_{zm} - h_{zp}); \tag{A5}$$

$$A_4 = \frac{u_{v1}}{2\lambda} - \frac{u_{v0}H_u}{2\lambda} - \left(\frac{H_{zu}}{2\lambda}\right)\left(w_{n0} + \frac{E_1 u_{v0}}{q_{20}\lambda}\right) - \frac{C_0 D_0}{\lambda} + \frac{3C_1 D_1}{\lambda}; \tag{A6}$$

$$\begin{gathered}\text{where } h_+ = h_p = \frac{k(\lambda+1)}{(8q_{10}q_{20}P_{1p})},\ \text{for } P_{1p} \neq 0;\ h_- = h_m = \frac{k(\lambda-1)}{(8q_{10}q_{20}P_{1m})}, \text{for } P_{1m} \neq 0;\\ h_+^* = h_{zp} = \frac{k\eta^2}{(q_{10}R_{1p})}, \text{for } P_{1p} \neq 0;\end{gathered} \tag{A7}$$

$$\begin{gathered}h_-^* = h_{zm} = \frac{k\eta^2}{(q_{10}R_{1m})},\ \text{for } R_{1m} \neq 0;\ H_u = \frac{\left((\lambda+2)h_p - (\lambda-2)h_m\right)}{2\lambda};\\ H_{zu} = \frac{1}{2}\left((\eta+1)h_{zp} - h_{zm}(\eta-1)\right);\end{gathered} \tag{A8}$$

$$B_3 = w_{n1} - \frac{D_2}{p_{20}} - \frac{D_3}{q_{20}(\eta^2-4)} - \frac{C_1 D_1}{q_{20}(\eta^2-10)} - \frac{B_1 H_{wm}}{4q_{20}} + \frac{2E_1 A_4}{q_{20}} - \frac{u_{v0}R_{wp}}{4\lambda q_{20}}, \text{for } \eta^2 \neq 4, \eta^2 \neq 10 \tag{A9}$$

$$B_4 = \frac{w_{v1}}{\eta} - \frac{B_2 H_{wp}}{4q_{20}\eta} - \frac{2E_2 A_3}{\eta q_{20}} + \frac{u_{n0}R_{wm}}{4\eta q_{20}}; \tag{A10}$$

$$H_{wp} = \frac{h_{zp}(\eta+2)}{\eta+1} - \frac{h_{zm}(\eta-2)}{\eta-1}, \text{for } \eta \neq 1 \tag{A11}$$

$$H_{wm} = \frac{h_{zp}}{\eta+1} - \frac{h_{zm}}{\eta-1},\ \text{for } \eta \neq 1 \tag{A12}$$

$$R_{1p} = \lambda^2 - (\eta+1)^2; \tag{A13}$$

$$R_{1m} = \lambda^2 - (\eta-1)^2; \tag{A14}$$

Initial values ($u(0) \equiv u_n$, $u'(0) \equiv u_v$, $w(0) \equiv w_n$, and $w'(0) \equiv w_v$) stand for the imposed non-dimensional displacement and its rate for the girder and the suspension. They are decomposed using two approximations in Equation (28).

The initial values for the first and second approximations are selected arbitrarily, and the corresponding constants are calculated. This establishes an iterative approach, where the true values of the constants are those that yield the dynamic equilibrium defined by Equation (31), satisfying the condition as $\delta_1(\xi) \to \delta_2(\xi) \to 0$, and ensuring the errors evaluated by Equation (32) are sufficiently small (e.g., of the order of 10^{-4}). Since $\varepsilon \ll 1$, in most cases, the correction of the initial values of the first approximation leads to the main influence for obtaining convergence, as the initial values of the second approximation contribute ε^{-1} times less to functions u and w. Furthermore, the initial values resulting

from the analytical solution should be satisfied, i.e., $u(0) \equiv u_n$, $u'(0) \equiv u_v$, $w(0) \equiv w_n$, and $w'(0) \equiv w_v$. In practical scenarios, when all the initial values for the girder and the vehicle suspension are zero, $A_1 = B_2 = A_3 = B_4 = 0$.

Appendix B. Numerical Solution of the Bridge–Vehicle Interaction

The following numerical solution for the explicit time-integration of the set of dynamic equations in Equation (3) is implemented. The solution is based on the implementation of the *5th-order Gear predictor–corrector* scheme, adopted here from molecular dynamics [25], yielding a very low artificial damping [26] effect in the simulation of spherical grain contact interaction [27] under combined slip and sliding motions [28].

Equation (3) is rewritten using resultant forces $F_C(t)$ and $F_V(t)$ acting on the lumped masses of the girder and moving vehicle suspension, respectively, where:

$$F_C(t) = \left(G_V - m_V \ddot{w}_V(t)\right) sin\theta t - k_C u_C(t) + F_c^{diss}(t), \tag{A15}$$

$$F_V(t) = k_V u_C(t) sin\theta t - k_V w_V(t), \tag{A16}$$

$F_c^{diss}(t) = -c_c \dot{u}_C$ is the girder's viscous damping force at t, which additionally accounts for evaluation of the effect of energy dissipation in the girder, $c_c = \zeta_c c_{c,crit}$, ζ_c is the bridge girder damping ratio of a critical damping to the damping of the girder, and $c_{c,crit} = 2m_C\omega_C$ is the critical damping of the girder.

The solution of Equation (3) at time t is performed *simultaneously* using the pre-defined array of time instants $t \in [0, t_1, \ldots, t + \Delta t, \ldots, L/c]$ by assuming that the time step is small enough at a minimum of a half-girder and at vehicle periods of free vibrations, i.e., $\Delta t \ll \pi min\left(\sqrt{m_v/k_v}, \sqrt{m_c/k_c}\right)$. All dynamical parameters of the bridge girder and vehicle suspension are denoted hereafter by the subscripts C and V, respectively. Meanwhile, the superscripts *pr* or *cr* specify the *prediction* and *correction* procedures of the solution.

The solution starts with initial boundary condition values $u_C(0)$, $\dot{u}_C(0)$, $\ddot{u}_C(0)$ and $w_V(0)$, $\dot{w}_V(0)$, $\ddot{w}_V(0)$, while all higher-order derivatives $b_{3C}^{pr}(0)$, $b_{4C}^{pr}(0)$, $b_{5C}^{pr}(0)$ and $b_{3V}^{pr}(0)$, $b_{4V}^{pr}(0)$, $b_{5V}^{pr}(0)$ are initially set to equal zero. These derivatives are collected during each time increment and ensure a higher accuracy of the prediction rather than the simple application of Taylor's series instead.

First, for any $t + \Delta t$, the unknown dynamical state variables of the girder—displacement $u_c \equiv x_c^{pr}$, velocity $\dot{u}_C \equiv v_C^{pr}$, acceleration $\ddot{u}_C \equiv a_C^{pr}$, and higher-order derivatives $b_{nc} = \frac{d^n x_c}{dt^n}\frac{\Delta t^n}{n!}$ (n = 3, 4, 5)—are pre-defined in the predictor procedure:

$$x_c^{pr}(t + \Delta t) = x_c(t) + \Delta t v_c(t) + \frac{1}{2}\Delta t^2 a_c(t) + b_{3c}(t) + b_{4c}(t) + b_{5c}(t), \tag{A17}$$

$$v_c^{pr}(t + \Delta t) = v_c(t) + \Delta t a_c(t) + \frac{1}{\Delta t}(3b_{3c}(t) + 4b_{4c}(t) + 5b_{5c}(t)), \tag{A18}$$

$$a_c^{pr}(t + \Delta t) = a_c(t) + \frac{2}{\Delta t^2}(3b_{3c}(t) + 6b_{4c}(t) + 10b_{5c}(t)), \tag{A19}$$

$$b_{3c}^{pr}(t + \Delta t) = b_{3c}(t) + 4b_{4c}(t) + 10b_{5c}(t), \tag{A20}$$

$$b_{4c}^{pr}(t + \Delta t) = b_{4c}(t) + 5b_{5c}(t), \tag{A21}$$

$$b_{5c}^{pr}(t + \Delta t) = b_{5c}(t), \tag{A22}$$

Then, the predicted mid-span displacement, its rate and higher order derivatives are corrected in the corrector procedure via a change in the accelerations:

$$\Delta a_c(t + \Delta t) = a_c(t + \Delta t) - a_c^{pr}(t + \Delta t), \tag{A23}$$

$$\text{where } a_C(t+\Delta t) = \frac{F_C\left(x_C^{pr}(t+\Delta t),\ v_C^{pr}(t+\Delta t),\ w_V(t)\right)}{m_C}, \tag{A24}$$

is the girder's lumped mass vertical motion acceleration, in which vehicle suspension dynamic displacement $w_V(t)$ is taken from preceding time instant t.

The *corrector procedure* corrects the predicted dynamic variables using $\Delta a_C(t + \Delta t)$:

$$\begin{pmatrix} x_C^{cr}(t+\Delta t) \\ v_C^{cr}(t+\Delta t) \\ a_C^{cr}(t+\Delta t) \\ b_{3C}^{cr}(t+\Delta t) \\ b_{4C}^{cr}(t+\Delta t) \\ b_{5C}^{cr}(t+\Delta t) \end{pmatrix} = \begin{pmatrix} x_C^{pr}(t+\Delta t) \\ v_C^{pr}(t+\Delta t) \\ a_C(t+\Delta t) \\ b_{3C}^{pr}(t+\Delta t) \\ b_{4C}^{pr}(t+\Delta t) \\ b_{5C}^{pr}(t+\Delta t) \end{pmatrix} + \begin{pmatrix} 0.5c_0\Delta t^2 \\ 0.5c_1\Delta t \\ c_2 \\ 0.5c_3\Delta t^2 \\ 0.5c_4\Delta t^2 \\ 0.5c_5\Delta t^2 \end{pmatrix} \Delta a_C(t+\Delta t), \tag{A25}$$

where $c_0 = 3/16$, $c_1 = 251/360$, $c_2 = 1.0$, $c_3 = 11/18$, $c_4 = 1/6$, and $c_5 = 1/60$ are the constants defining accuracy for a second-order differential equation [27].

All dynamical parameters computed in the corrector procedure give the final solution at any $t + \Delta t$ for the girder dynamic variables: $u_C \equiv x_C^{cr}$, $\dot{u}_C \equiv v_C^{cr}$, $\ddot{u}_C \equiv a_C^{cr}$, $b_{nC} \equiv b_{nC}^{cr}$ ($n = 3, 4, 5$).

Next, in the same way, the dynamic variables of the vehicle suspension—$w_V \equiv x_V^{pr}$, $\dot{w}_V \equiv v_V^{pr}$, $\ddot{w}_V \equiv a_V^{pr}$, and b_{nV}^{pr} ($n = 3, 4, 5$)—are computed in the predictor procedure by taking all the dynamic resolved variables of the girder. Thus, the second dynamic equation of set (3) is resolved by simply setting subscript C=V and applying the suspension resultant force (A16), substituting $u_C^{cr}(t + \Delta t)$ and its rate $\dot{u}_c^{cr}(t + \Delta t)$.

For a new time instant, all the resolved variables of the girder and vehicle suspension in the corrector procedure are substituted in the predictor procedure, while the calculation loop is repeated in the same manner. The numerical solution ends when $t = L/c$ and the vehicle passes the girder.

The correctness and accuracy of the numerical solution have also been verified vs. a variable order multistep Adams–Bashforth–Moulton method [29]. This approach is normally applied when stringent tolerances of errors are required. Contrary to the implemented prediction–correction approach, accuracy in the Adams–Bashforth–Moulton method is gained by referring linearly to several previous time instants and function derivative values. In terms of verification of correctness of numerical analysis, for solution via the Adams–Bashforth–Moulton method, an intrinsic Matlab solver ode113 was used with relative error tolerance values 1E-12 selected. As the solver operates only with first-order differential equations, Equation (3) was rewritten in the following set of four differential equations:

$$\begin{cases} \dot{v}_C = \frac{1}{m_C}((G_V - k_V(u_C sin\theta t - w_V))sin\theta t - k_C u_C), \\ \dot{v}_V = \frac{1}{m_V}(k_V u_C sin\theta t - k_V w_V), \\ v_C = \dot{u}_C, \\ v_V = \dot{w}_V. \end{cases}$$

In Figure A1, the results of a full coincidence of numerical solution of Equation (3) using the implemented 5th order Gear predictor–corrector approach and Adams–Bashforth–Moulton method are demonstrated. The proposed approximate analytical solution (denoted by subscript *th*) results in very small deviations in comparison with numerical solution results. Detailed analysis of analytical predictions was considered in Section 5.

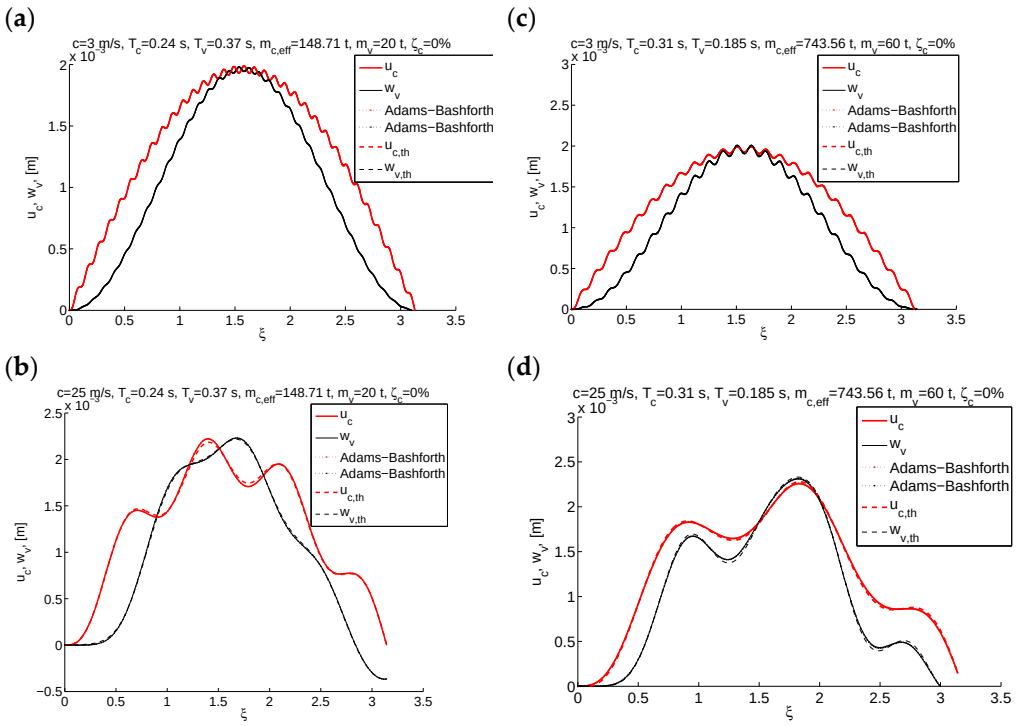


Figure A1. Evolution of girder mid-span and vehicle suspension vertical displacements for different cases of girder, vehicle, and loading frequencies vs. dimensionless time: (**a**,**b**) $\omega_C + \theta > \omega_V$; (**c**,**d**) $\omega_C + \theta < \omega_V$.

References

1. Yang, Y.B.; Liu, Y.H.; Xu, H. Recovering mode shapes of curved bridges by a scanning vehicle. *Int. J. Mech. Sci.* **2023**, *253*, 108404. [CrossRef]
2. Massarelli, E.; Civera, M.; Mara, S.; Raimondi, M.; Giordano, P.F.; Quqa, S.; Aimar, M.; Limongelli, M.P.; Chiaia, B. Crowdsensing-based automated operational modal analysis for indirect bridge structural health monitoring. *Eng. Struct.* **2026**, *353*, 122203. [CrossRef]
3. Massarelli, E.; Raimondi, M.; Mara, S.; Civera, M.; Aimar, M.; Giordano, P.F.; Coletta, D.; Chiola, D.; Carambia, B.; Limongelli, M.P.; et al. Output-only modal analysis and system identification for indirect bridge health monitoring: Needs, requirements, and limitations. In *Proceedings of the 10th International Operational Modal Analysis Conference (IOMAC 2024)*; Springer: Cham, Switzerland, 2024; Volume 2.
4. Mazzeo, M.; Di Matteo, A.; Santoro, R. An enhanced indirect modal identification procedure for bridges based on the dynamic response of moving vehicles. *J. Sound Vib.* **2024**, *589*, 118540. [CrossRef]
5. Zhang, T.; Xiong, Z.; Zhu, J.; Zheng, K.; Wu, M.; Li, Y. Extracting bridge frequencies from the dynamic responses of moving and non-moving vehicles. *J. Sound Vib.* **2023**, *564*, 117865. [CrossRef]
6. Qu, C.-X.; Liu, C.-C.; Yi, T.-H.; Li, H.-N. Response prediction of lumped mass structures based on physical parameter identification through experimental modal analysis. *J. Eng. Mech.* **2026**, *152*, 04026013. [CrossRef]
7. Liu, Y.-F.; Qu, C.-X.; Yi, T.-H.; Li, H.-N.; Zhai, B.-Z. Modal parameters identification of highly non-orthogonal structures based on curve fitting frequency domain decomposition method. *Eng. Struct.* **2026**, *357*, 122545. [CrossRef]
8. Yang, Y.B.; Zhang, B.; Wang, T.; Xu, H.; Wu, Y. Two-axle test vehicle for bridges: Theory and applications. *Int. J. Mech. Sci.* **2019**, *152*, 51–62. [CrossRef]
9. Fryba, L. *Vibration of Solids and Structures Under Moving Loads*; Thomas Telford: London, UK, 1999; 485p.
10. Fryba, L. Dynamic interaction of vehicles with tracks and roads. *Veh. Syst. Dyn.* **1987**, *16*, 129–138. [CrossRef]
11. Mackertich, S. Moving load on a Timoshenko beam. *J. Acoust. Soc. Am.* **1990**, *88*, 1175–1178. [CrossRef]
12. Mackertich, S. Response of a beam to a moving mass. *J. Acoust. Soc. Am.* **1992**, *92*, 1766–1769. [CrossRef]
13. Foda, M.A.; Abduljabbar, Z. A dynamic Green function formulation for the response of a beam structure to a moving mass. *J. Sound Vib.* **1998**, *210*, 295–306. [CrossRef]
14. Olsson, M. On the fundamental moving load problem. *J. Sound Vib.* **1991**, *145*, 299–307. [CrossRef]
15. Pesterev, A.V.; Bergman, L.A.; Tan, C.A.; Tsao, T.C.; Yang, B. On asymptotics of the solution of the moving oscillator problem. *J. Sound Vib.* **2003**, *260*, 519–536. [CrossRef]

16. Erdelyi, A.; Magnus, W.; Oberhettinger, F.; Tricomi, F.C. *Higher Transcendental Functions*; McGraw-Hill book Co., Inc.: New York, NY, USA, 1955; Volume 3, 292p.
17. Whittaker, E.T.; Watson, G.N. *A Course of Modern Analysis. An Introduction to the General Theory of Infinite Processes and of Analytic Functions with an Account of the Principal Transcendental Functions*; Cambridge University Press: Cambridge, UK, 1996; 608p.
18. Polyanin, A.D.; Zaitsev, V.F. *Handbook of Exact Solutions for Ordinary Differential Equations*; CRC Press: Boca Raton, FL, USA, 2003; 782p.
19. Daniel, D.J. Exact solutions of Mathieu's equation. *Prog. Theor. Exp. Phys.* **2020**, *2020*, 043A01. [CrossRef]
20. Balevičius, R.; Mróz, Z. Relative transverse slip and sliding of two spherical grains in contact. *J. Eng. Mech. ASCE* **2019**, *145*, 04019012. [CrossRef]
21. Rand, R.H. Lecture notes of nonlinear vibrations. In *Department of Theoretical & Applied Mechanics*; Cornell University Department Theoretical & Applied Mechanics: Ithaca, NY, USA, 2003; p. 111.
22. Kovacic, I.; Rand, R.; Sah, S.M. Mathieu's equation and its generalizations: Overview of stability charts and their features. *Appl. Mech. Rev.* **2018**, *70*, 020802. [CrossRef]
23. McLachlan, N.W. *Theory and Application of Mathieu Functions*; Clarendon Press: Oxford, UK, 1947; 401p.
24. Clough, R.W.; Penzien, J. *Dynamics of Structures*; Computers & Structures, Inc.: Walnut Creek, CA, USA, 2003; 730p.
25. Allen, M.P.; Tildesley, D.J. *Computer Simulation of Liquids*; Clarendon Press: Oxford, UK, 1991.
26. Balevičius, R.; Kačianauskas, R. DEM analysis of granular flow in pyramidal hoppers. In *Proceedings III European Conference on Computational Mechanics. Solids, Structures and Coupled Problems in Engineering*; Springer: Dordrecht, The Netherlands, 2006.
27. Balevičius, R.; Kačianauskas, R.; Džiugys, A.; Maknickas, A.; Vislavičius, K. Investigation of performance of programming approaches and languages used for numerical simulation of granular material by the discrete element method. *Comput. Phys. Commun.* **2006**, *175*, 404–415. [CrossRef]
28. Balevičius, R.; Mróz, Z. A finite sliding model of two identical spheres under displacement and force control. Part II: Dynamic analysis. *Acta Mech.* **2014**, *225*, 1735–1759. [CrossRef]
29. Shampine, L.; Gordon, M. *Computer Solution of Ordinary Differential Equations: The Initial Value Problem*; W. H. Freeman: San Francisco, CA, USA, 1975.

Disclaimer/Publisher's Note: The statements, opinions and data contained in all publications are solely those of the individual author(s) and contributor(s) and not of MDPI and/or the editor(s). MDPI and/or the editor(s) disclaim responsibility for any injury to people or property resulting from any ideas, methods, instructions or products referred to in the content.